A critical period for prefrontal cortex PV interneuron myelination and maturation

S. Hijazi[1,2], M. Pascual-García[1], Y. Nabawi[1], S.A. Kushner[1]

[1] Department of Psychiatry, Erasmus MC, Rotterdam, The Netherlands
[2] Department of Pharmacology, University of Oxford, Oxford, UK

Abstract

Recent studies have highlighted axonal myelination as a common feature of PV interneurons throughout the cerebral cortex. However, the precise function of PV interneuron myelination remains incompletely understood. In this study, we used the cuprizone model of demyelination to investigate how PV interneuron myelination might influence their neuronal physiology. Specifically, we examined whether impairing myelination from postnatal day 21 onwards, during a critical neurodevelopmental period of the prefrontal cortex (PFC), can affect PV interneuron maturation and function. Using whole-cell patch-clamp recordings to examine intrinsic properties of PV interneurons in the PFC, we found that juvenile demyelination induced robust alterations of PV interneuron firing patterns. Specifically, we observed that demyelination caused an impairment in the ability of PV interneurons to sustain high frequency firing associated with a substantial decrease in Kv3-specific currents. We also found a significant impairment in PV interneurons autaptic self-inhibitory transmission, a feature implicated in temporal control of PV interneurons firing during cortical network activity. Following a remyelination period of 5 weeks, PV interneuron properties were only partially recovered and mice showed clear social deficits, suggesting that transient juvenile demyelination leads to long-lasting behavioral impairments. In contrast, adult demyelination had no effect on PV interneuron firing properties or autaptic plasticity. Together, our data uncovers a critical period for juvenile myelination as an important factor in PFC PV interneuron development and brain maturation.

Introduction

Cortical parvalbumin (PV) interneuron properties develop rapidly during the third postnatal week. PV interneurons, also known as fast-spiking interneurons, start showing their unique and mature features, such as a narrow action potential (AP) waveform and high frequency firing, during a specific postnatal time window, extending between postnatal day (P)14 and P28, which depends on the developmentally-regulated expression of a specific complement of voltage-gated ion channels [1–3]. Another important developmental aspect of PV interneurons is their extensive myelination which emerges in parallel around P15[3–5]. While the role of myelination has been widely studied in long-range projection neurons, the impact of

myelination on local PV cortical interneurons is still poorly understood. Recent studies have endorsed the classical view that myelination of PV interneurons should function to increase axonal conduction velocity in a similar manner as has been well demonstrated in many other neuronal subtypes[6], while also being critical for PV interneuron-mediated feedforward inhibition in cortical sensory circuits [7]and modulation of local circuit synchronization[8]. Interestingly, impairing PV neuronal-glial interactions during development was shown to alter myelination patterns in PV interneurons and reduce their firing rate [7,9]. Yet, the specific role of PV interneuron myelination over the time course of neurodevelopment has yet to be elucidated.

Aberrant PV interneuron maturation has been suggested as a key player in the pathogenesis of various neurodevelopmental diseases, and impairment in the development of prefrontal cortex (PFC) circuits has been at the center of many studies investigating neurodevelopmental disorders[10–14]. Hence, the maturation of PV interneurons in PFC is of particular significance. Notably, PFC development persists long after adolescence[13,15] and PFC-dependent functions, such as cognitive flexibility and emotional memory encoding, start emerging later in development[13,15]. PFC maturation is hence delayed compared to other cortical regions and it is only in adulthood that PFC becomes fully developed and acts as a hub for cognitive processing[16]. This delayed period of maturation of PFC circuits underlies an important time window necessary for the establishment of specific neuronal circuits within the PFC[16–18]. Conversely, it also reveals a transient period during which the PFC is vulnerable to various types of stressors and insults[17].

Here, we investigated whether juvenile demyelination, starting at P21, can impair PV interneuron maturation in the PFC. Our data revealed that myelination of PV interneurons during this critical period of development is instrumental for PV interneuron maturation and their unique ability to fire at high frequencies. We show that juvenile demyelination can have long lasting effect on PV interneuron morphology and function and impair social behavior in adulthood.

Results

Juvenile demyelination affects PV interneuron properties, maturation and morphology in PFC

In order to investigate whether demyelination during the critical period of PFC maturation would impair PV interneuron maturation and function, mice were fed a 0.2% cuprizone diet for 6 weeks starting at P21. Mice were then sacrificed and brain slices were prepared for whole-cell patch-clamp recording and filling of PV interneurons (**Figure 1A**). Juvenile cuprizone treatment led to a clear decrease in myelination in adulthood and to a complete demyelination

of PV interneuron axons in the PFC (**Figure 1B-C**). Next, we fully reconstructed the biocytin-filled patched cells and quantified their axonal and dendritic processes (**Figure 1D-E**). We found a significant decrease in the total axonal length and the number of axonal branching points of PV interneurons from mice th at underwent juvenile demyelination when compared to control mice (**Figure 1F**) while the total dendritic length was unaffected (**Figure 1G**). The total number of PV interneurons was unaltered by juvenile demyelination (**Figure 1H-I**).

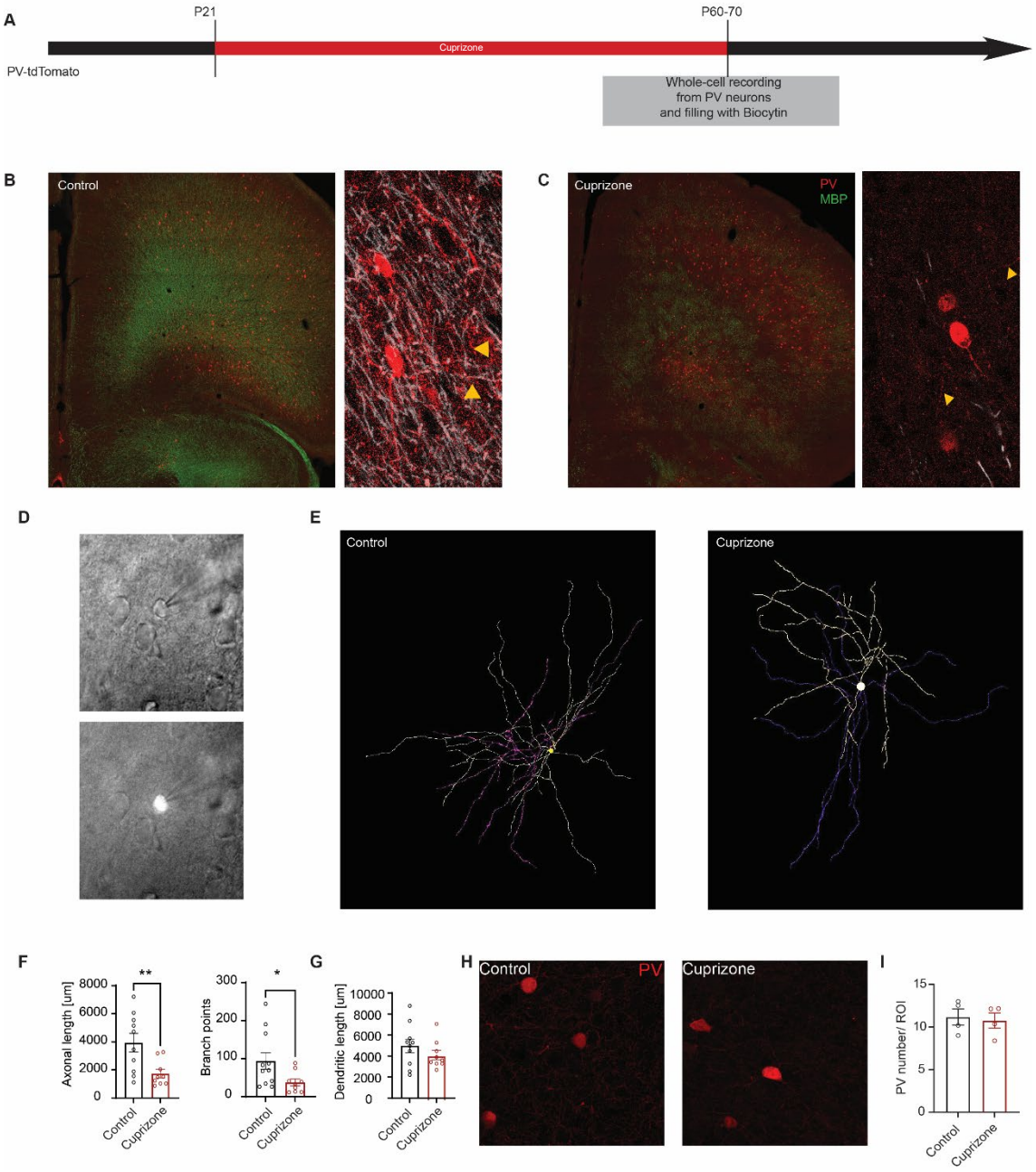

Figure 1. Juvenile demyelination leads to a decrease in axonal complexity of PFC PV interneurons. A. Experimental design to induce juvenile demyelination in PV-tdTomato mice **B.** *Left.* Confocal overview image of PFC in PV-tdTomato animal (tdTomato+, red) overlaid with myelin basic protein (MBP, green). *Right*. 40x image showing myelinated PV interneuron axons in control conditions. **C**. *Left.* Confocal overview image of the PFC region immunolabeled for MBP expression showing the loss of myelin following 6 weeks of 0.2% cuprizone-diet. *Right*.

40x image showing no myelination of PV interneuron axons in cuprizone conditions. Yellow arrow heads point to PV interneuron axons. **D**. Live contrast image (upper) of a tdTomato-labeled (lower) PV interneuron in the PFC region with the patch pipette attached. **E**. Example image of a fully reconstructed biocytin-labeled PFC PV interneuron from a control mouse (left) and from cuprizone-treated mouse (right). **F**. *Left*. Total proximal axonal length is decreased in cuprizone-treated PFC PV interneurons compared with control cells (*t-test; n = 10/9 cells per group, **p < 0.01). Right*. The number of branch points in PV interneuron axons from cuprizone-treated mice was significantly decreased compared to control mice (*t-test; n = 10/9 cells per group, *p < 0.05*). **G**. Total dendritic lengths was unaltered by juvenile demyelination (*t-test; n = 10/9 cells per group, p = 0.2856*). **H.** PV interneurons were visualized in coronal sections of the PFC of control (left panel) and cuprizone-treated (right panel) mice using anti-PV staining (red). The number of PV-positive cells was quantified in high magnification images. **I**. Quantification of the total number of PV interneurons in the PFC region shows no difference between control (black) and cuprizone-treated (red) mice (*t-test; n = 4 mice per group, p = 0.7577*).

Given that demyelination during adolescence led to a significant change in PV interneuron's morphology, we next aimed to characterize whether juvenile demyelination affected PV interneurons intrinsic and firing properties. To that end, we performed current clamp recordings from PFC PV interneurons following juvenile demyelination. Our data revealed alterations in both passive and active membrane properties of PFC PV interneurons in mice that underwent juvenile demyelination, all indicative of an immature PV interneuron phenotype (**Figure 2**). Specifically, there was a significant increase in the input resistance and sag amplitude, with a trend towards a more depolarized resting membrane potential (**Figure 2A-F**). The action potential (AP) waveform was also affected by cuprizone treatment (**Figure 2G**), showing a substantial increase in AP width, decay time and afterhyperpolarization (AHP) duration (**Figure 2I-L**). Furthermore, there was a significant decrease in the firing frequency of PV interneurons from cuprizone mice, along with an impairment in the maximum firing frequency (**Figure 2M-O**). Strikingly, the difference in firing frequency was apparent from 50 Hz onwards (**Figure 2N**) and 38.4% (20 out of 52) of PV interneurons from the cuprizone group could not sustain their firing throughout the entire 500 ms window of high current injection, while only 11.6% (5 out of 43) of the cells from the control group showed a similar phenotype (**Figure 2P-Q**). Interestingly, PV interneurons from the primary somatosensory cortex (S1) did not show any impairment in high-frequency firing. Only 1 of the 54 cells recorded in S1 was unable to sustain high-frequency firing (**Supplementary Figure 1**). Taken together, these data suggest that juvenile demyelination impairs PV interneuron maturation in the PFC.

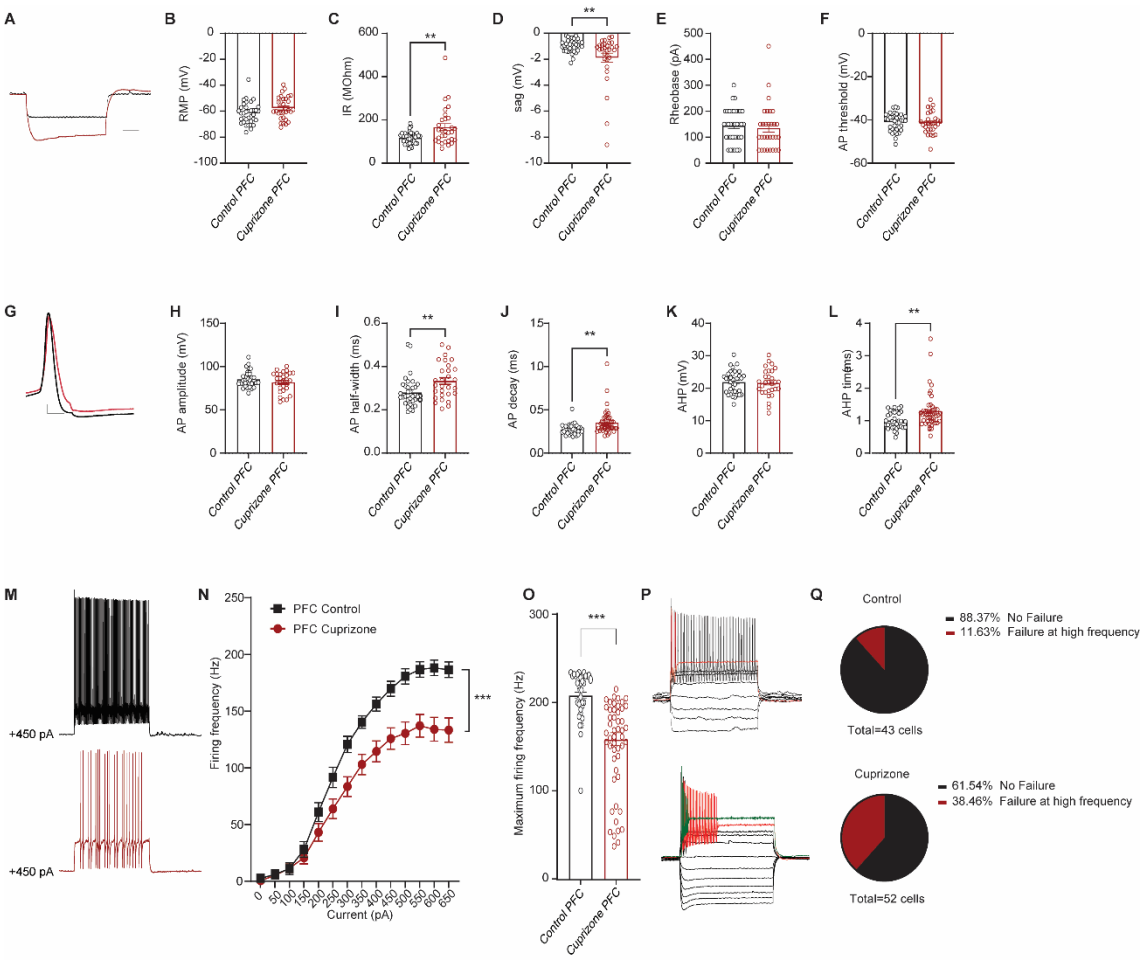

Figure 2. Juvenile demyelination impairs the maturation of PV interneurons in the PFC. **A**. Representative traces of voltage responses following a hyperpolarizing step from control (black) and cuprizone-treated (red) mice illustrating an increased input resistance and sag in mice that underwent juvenile demyelination. **B**-**F**. Summary data showing the averaged (± s.e.m) of the following intrinsic properties: (B) Resting membrane potential (RMP) (*t-test; n = 36/30 cells from 9/8 mice per group, p = 0.0511*), (C) Input resistance (IR) (*t-test; n = 36/30 cells from 9/8 mice per group, **p < 0.01*), (D) Sag (*t-test; n = 36/30 cells from 9/8 mice per group, **p < 0.01*), (E) Rheobase (*t-test; n = 36/30 cells from 9/8 mice per group, p = 0.6853*) and (F) Action potential (AP) threshold (*t-test; n = 36/30 cells from 9/8 mice per group, p = 0.7831*). **G**. A representative trace of a single AP illustrating a wider and slower AP in cuprizone-treated mice (red) compared to control (black) . **H**-**L**. Summary data showing the averaged (± s.e.m) of the following AP waveform properties: (H) AP amplitude (*t-test; n = 36/30 cells from 9/8 mice per group, p = 0.1534*), (I) AP half-width (*t-test; n = 36/30 cells from 9/8 mice per group, **p < 0.01*), (J) AP decay (*t-test; n = 36/30 cells from 9/8 mice per group, **p < 0.01*), (K) After-hyperpolarization (AHP) amplitude (*t-test; n = 36/30 cells from 9/8 mice per group, p = 0.7903*) and (L) AHP time (*t-test; n = 36/30 cells from 9/8 mice per group, **p < 0.01*). **M**. Representative traces of voltage responses following +450 pA current injection. **N**. Average action potential (AP) frequency in response to 0-650 pA current steps illustrating a significant decrease in PV interneuron firing frequency in cuprizone-treated mice. (*group x current two-way repeated measures: n = 36/30 cells from 9/8 mice per group: F(13,836)= 4.00, p < 0.001*). **O**. Summary data of the maximum firing frequency per group (*t-test; n = 36/30 cells from 9/8 mice per group, ***p < 0.001*). **P**. Example traces of two different PV interneurons that are unable to maintain high-frequency firing at increased current injection. The upper trace shows a cell that can sustain its firing at low-current but not at high, whereas the lower trace shows a cell that can't sustain its firing at any current-step. **Q**. Percentage of cells that failed to maintain high

frequency firing at > 500 pA in both groups reveals a clear increase in cuprizone-treated mice (*Fisher's exact test; **p = 0.0045*). Data was obtained from voltage recordings with 500 ms current injections ranging from -300 pA to 650 pA.

Juvenile demyelination induces a loss of functional autapses and impairs autaptic plasticity at high frequencies

Recent studies have supported a role for autapses, synaptic inputs from one PV interneuron onto itself, in the ability of these cells to control network oscillations and have been suggested to play a role in the fast-spiking abilities of PV interneurons [18-20]. Accordingly, in the next set of experiments, we set out to explore whether juvenile demyelination caused changes in autaptic transmission, possibly underlying the observed impairments in firing frequency at high current injections. To that end, we recorded inhibitory autaptic postsynaptic responses in PFC PV interneurons at P60-75 (**Figure 3A**). There was a significant decrease in PV interneurons showing an autaptic response in the cuprizone group (53.8%; 28 out of 52) compared to the control group (75.9%; 44 out of 58) (**Figure 3B**). We observed comparable results in PV interneurons from S1, where 48.2% (26 out of 54) of the cells had no autaptic response following juvenile demyelination compared to only 16.1% (5 out of 31) in the control group, highlighting a critical role for juvenile myelination in maturation of autaptic responses (**Supplementary Figure 2**). Next, we went to back to the reconstructed cells and examined whether they had structural autapses, i.e. a colocalization between the axon of one cell and soma/dendrite of the same cell. 29.2% of PV interneurons from cuprizone mice and 11.8% from control mice had no morphological autapses (**Figure 3C-D**). Interestingly, in the cuprizone group, 25.0% of the cells had morphological autapses but showed no autaptic response, indicating that juvenile demyelination led to a loss of functional autapses and an increase in failures of autaptic responses. We then investigated whether the remaining PV interneurons, which had both structural autapses and an autaptic response (45.8%), showed any other impairments in autaptic transmission. We did not observe any significant changes in the amplitude or decay of the autaptic response (**Figure 3E-G**). In view of the observed impaired firing at high frequencies in current clamp recordings, we next questioned whether high-frequency induced plasticity at autaptic sites is also affected by juvenile demyelination. Subsequently, in voltage-clamp mode, we performed 100 AP trains of voltage commands at 200 Hz. Notably, in control mice the paired autaptic response (IPSC2/1) showed a clear facilitation (**Figure 3H-I**). In cuprizone-treated mice, however, most PV interneurons did not show any plasticity at 200 Hz (**Figure 3H-I**). Moreover, we noted a significant increase in failure rate in subsequent autaptic responses when AP trains where evoked at this frequency (**Figure 3J-K**).

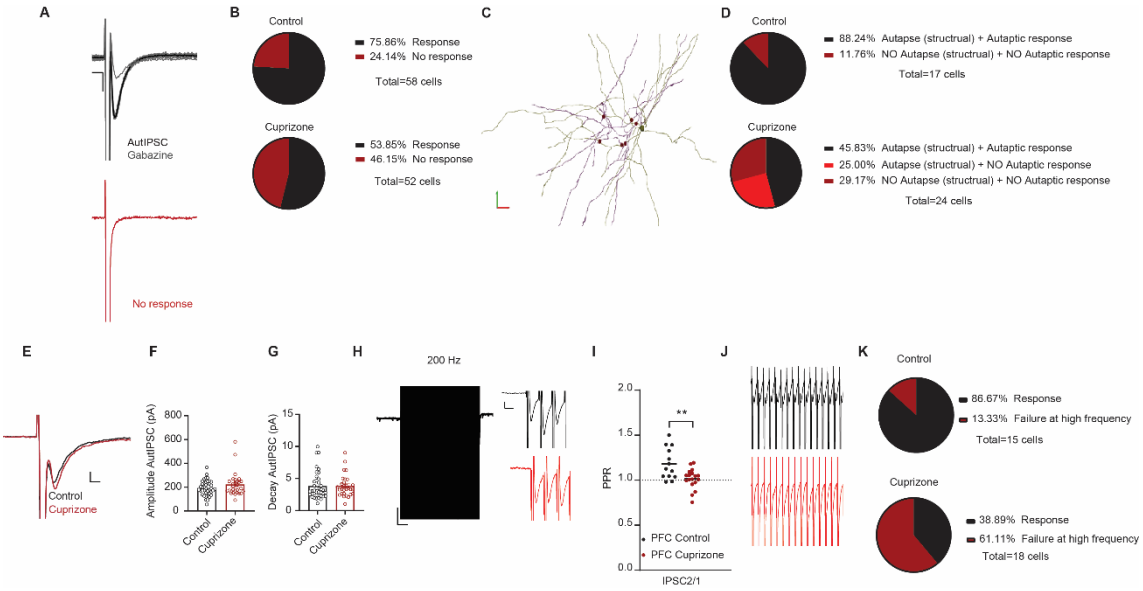

Figure 3. Juvenile demyelination induces a loss of functional autapses. A. *Upper panel*. Example traces (average of 8 sweeps) of unitary autaptic inhibitory postsynaptic currents triggered by voltage steps from holding potential of- 70mV to 0 mV in PV interneuron (fast inward Na+ currents were partially removed), which can be blocked by gabazine (grey). Note the expected fixed latency for all single-trial responses. *Lower panel*. Example trace showing a failure in autaptic response. scale: 100 pA, 5ms **B**. Cuprizone-treated mice show a significant decrease in the percentage of cells showing an autaptic response (*Fisher's exact test; *p = 0.0173*). **C**. An example image of a PFC PV interneuron fully reconstructed using Neurolucida showing autapses in red circles. Note that all autapses are present in a close distance from the soma. **D**. Pie charts depicting the percentage of cells showing (1) both structural and physiological autapses, (2) no structural nor physiological autapses and (3) only structural autapses. Note that only mice that underwent juvenile demyelination have PV interneurons which show structural autapses but no autaptic response. **E**. Example traces of an autaptic response in control (black) and cuprizone (red). scale:100 pA, 5ms. **F**-**G**. There was no difference between groups in the amplitude (**F**) or decay (**G**) of the autaptic post-synaptic currents in cells that had autapses (*t-test; n = 40/28 cells per group, p = 0.1246 (F) and p = 0.9350 (G)*). **H.** *Left.* Example trace of the train of 100 AP at 200 Hz in voltage-clamp mode. *Right.* Inset of of the first three unitary autaptic IPSCs in a train of 100 evoked at 200 Hz in PFC PV interneurons from control mice (black) and cuprizone-treated mice (red) ; Note the clear facilitation in the second response in the control mice . **I**. Quantification of the paired-pulse ratio (PPR) of both control (black dots) and cuprizone-treated (red dots) mice reveal an impairment in short-term plasticity at autaptic site following juvenile demyelination (*t-test: n =13,18 cells from 7-8 mice per group, **p = 0.0072*). **J.** Example traces of the first 15 unitary autaptic IPSCs in a train of 100 evoked at 200 Hz in PFC PV interneurons from control mice (black) and cuprizone-treated mice (red) ; Note that many evoked responses failed in the cuprizone mice . **K**. Cuprizone-treated mice show a significant increase in the percentage of cells showing a failed autaptic response at 200 Hz (*Fisher's exact test; *p = 0.0110*).

Loss of PV interneuron autapses increases their likelihood to show impaired firing at high frequency

Our results so far seem to suggest a link between the loss of functional autapses and the impaired firing rate that we observed in PV interneurons following juvenile demyelination. We were therefore interested in exploring further whether the presence of autapses could affect PV interneuron properties and firing rate. To that end, we divided the cells from both groups

into (1) cells that had an autaptic response and (2) cells that had no autaptic response (**Supplementary Figure 3**). In the control group, we found that PV interneurons with no autapses (24.1%) were more excitable than those that had autapses, with a difference in rheobase of ~40 pA (**Supplementary Figure 3A,B**). PV interneurons with no autapses also showed a decreased AHP and no changes in AP width (**Supplementary Figure 3C,D**). Importantly, these cells had an increased firing rate following low-current injections (0-250 pA) but at high-current, their frequency was decreased compared to cells that had autapses (**Supplementary Figure 3E**). Additionally, cells without autapses had a lower maximum firing frequency compared to cells with autapses (**Supplementary Figure 3F**). These data validate the importance of autapses for high-frequency firing in PV interneurons. In fact, in mice that underwent juvenile demyelination, 60.0% (18 out of 30)of PV interneurons that had no autaptic response showed impaired firing. Conversely, 60.0% (12 out of 20) of PV interneurons with impaired firing had no autaptic response (**Supplementary Figure 3G-H**), suggesting that the absence of autapses in the juvenile demyelination group increased the likelihood of PV interneurons exhibiting impaired firing. Indeed, 31.0% (16 out of 52)of all PV interneurons from the cuprizone group showed both no autaptic responses and an impaired firing phenotype versus only 4.6% (2 out of 43) in the control group. It is interesting to note that in juvenile demyelination mice, there was no substantial difference in maximum firing frequency when comparing cells with autapses to cells without autapses (**Supplementary Figure 3F**).

Remyelination in adulthood can only partially restore PV interneuron properties in the PFC

Our data has revealed a clear impairment in PV interneuron properties and self-inhibitory transmission following juvenile demyelination. We next questioned whether remyelination could fully restore PV interneuron function in PFC. To that end, we exposed mice to juvenile demyelination from P21 to P60, and then the cuprizone food was replaced with control food from P60 to P100 (**Figure 4A-B**). We then performed whole-cell recordings from PV interneurons in the PFC.

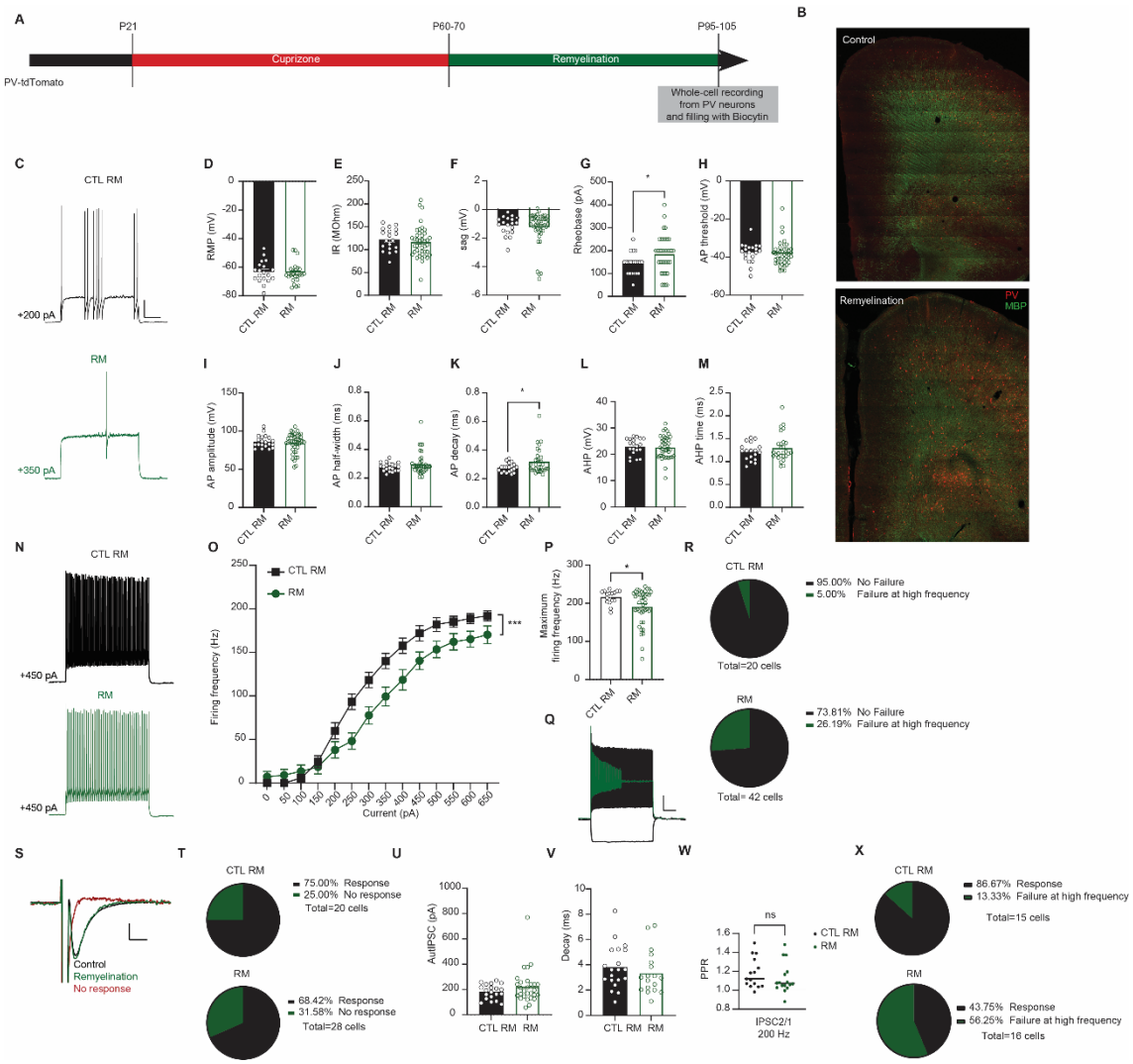

Figure 4. Remyelination in adulthood leads to an incomplete restoration of PV interneuron properties. A. Experimental design for remyelination in PV-tdTomato mice **B**. *Upper panel*. Confocal overview image of PFC in PV-tdTomato animal (tdTomato+, red) overlaid with myelin basic protein (MBP, green). *Lower panel*. Confocal overview image immunolabeled for MBP expression showing remyelination of the PFC region following 5 weeks of normal diet. **C**. Representative traces of voltage responses following a depolarizing step from control (black) and remyelination (green) mice illustrating an increased in Rheobase in mice after remyelination. Scale: 20 mV, 100ms. **D**-**H**. Summary data showing the averaged (± s.e.m) of the following intrinsic properties: (D) Resting membrane potential (RMP) (*t-test; n = 25/19 cells from 8 mice per group, p = 0.7435*), (E) Input resistance (IR) (*t-test; n = 25/19 cells from 8 mice per group, p = 0.5626*), (F) Sag (*t-test; n = 25/19 cells from 8 mice per group, p = 0.6088*), (G) Rheobase (*t-test; n = 25/19 cells from 8 mice per group, *p < 0.05*) and (H) Action potential (AP) threshold (*t-test; n = 25/19 cells from 8 mice per group, p = 0.6472*). **I**-**M**. Summary data showing the averaged (± s.e.m) of the following AP waveform properties: (I) AP amplitude (*t-test; n = 25/19 cells from 8 mice per group, p = 0.4951*), (J) AP half-width (*t-test; n = 25/19 cells from 8 mice per group, p = 0.2202*), (K) AP decay (*t-test; n = 25/19 cells from 8 mice per group, *p < 0.05*), (L) After-hyperpolarization (AHP) amplitude (*t-test; n = 25/19 cells from 8 mice per group, p = 0.8156*) and (M) AHP time (*t-test; n = 25/19 cells from 8 mice per group, p = 0.3123*). **N**. Representative traces of voltage responses following +450 pA current injection. **O**. Average action potential (AP) frequency in response to 0-650 pA current steps illustrating a significant decrease in PV interneuron firing frequency in remyelination (green) mice (*group x current two-way repeated measures: n = 25/19 cells from 8 mice per group: F(13,546)= 3.962, ***p < 0.001*). **P**. Summary data of the maximum firing frequency per group

(*t-test; n = 25/19 cells from 8 mice per group, *p < 0.05*). **Q**. Example trace of a PV interneuron that is unable to maintain high-frequency firing at increased current injection. **R**. Percentage of cells that failed to maintain high frequency firing at > 500 pA is still not fully recovered after remyelination (*Fisher's exact test; p = 0.0828*). **S**. Representative voltage steps showing an AutIPSC response in control (black) and remyelination (green) groups. The red trace shows a cell that had NO autaptic response. Scale: :50 pA, 2ms. **T**. Remyelination mice show no difference in the percentage of cells showing an autaptic response compared to control mice (*Fisher's exact test; p = 0.7639*). **U-V**. There was no difference between groups in the amplitude (U) or decay (V) of the autaptic post-synaptic currents in cells that had autapses in the remyelination group (green) compared to the control group (black) (*t-test; n = 28/20 cells from 8 mice per group, p = 0.1939 (U) and p = 0.4328 (V)*). **W-X**. Paired-pulse ratio (PPR) of both control (black dots) and remyelination (green dots) mice shows no difference in short-term plasticity at autaptic sites specifically at 200 Hz (*t-test; n = 15/16 cells from 8 mice per group, p = 0.3388*). Yet, the percentage of cells showing a failed autaptic response at 200 Hz remains increased in the remyelination group compared to the control group (Fisher's exact test; *p = 0.0233).

Interestingly, we found that remyelination caused a significant increase in the rheobase of PV interneurons, promoting a decreased excitability of these cells. Both the input resistance and the sag amplitude were fully restored to control levels upon remyelination (**Figure 4C-H**). When examining the AP waveform, we detected a small increase in the decay of the AP in the remyelination group, even though AP half-width was not significantly different (**Figure 4I-M**). PV interneurons from the remyelination group still showed decreased firing frequency in response to increased current injections (**Figure 4N-P**). Even after remyelination, 26.2% (11 out of 42) of the cells still could not sustain their firing at high frequency, compared to 5.0 %(1 out of 20) in control mice (**Figure 4Q,R**). These results suggest that remyelination leads to a partial rescue of PFC PV interneurons. However, the impairment is still apparent when PV interneurons are driven to fire at high frequencies. Remarkably, remyelination does fully rescue PV properties in S1 (**Supplementary Figure 4**), indicating that juvenile demyelination has long-lasting effects on PV interneuron firing properties specifically in the PFC. We then investigated self-inhibitory transmission was restored by remyelination (**Figure 4S-X**). Remyelination resulted in a rescue of autaptic neurotransmission, as the percentage of the cells showing an autaptic responses (68.4%; 19 out of 28) was not statistically different from control mice (75.0%; 15 out of 20) (**Figure 4S-T**). The amplitude and decay of the responses were also not different across groups (**Figure 4U,V**). As juvenile demyelination impaired short-term plasticity at autaptic sites, we next examined whether remyelination could also restore autaptic plasticity. No significant difference between the two groups was detected in short-term plasticity at 200 Hz and almost all cells from the remyelination group showed paired pulse facilitation (**Figure 4W**). Yet, there was a significant difference in the percentage of cells that showed failed responses at 200 Hz in the remyelination group compared to the control one (**Figure 4X**). These data point to a rescue of autaptic plasticity upon remyelination, albeit not all the parameters were fully restored.

Juvenile demyelination has long-lasting effects on social behavior

As previous studies have demonstrated that impaired myelination during this critical period leads to impaired social behavior in adulthood[22], we next explored whether cuprizone mice, that underwent a period of juvenile demyelination followed by remyelination, have any deficits in social behavior (**Figure 5**). More specifically, we were interested to examine whether the impairments in PV interneuron properties at high frequencies might be associated with behavioral changes. To that end, we performed a social behavior test, the three-chamber test, which is associated with PFC function. In the first phase of the test, sociability was assessed (preference of mouse over object). Mice that had undergone juvenile demyelination followed by a period of remyelination showed no preference towards the mouse compared to the object, while control mice spent significantly more time exploring the mouse compared to the object (**Figure 5B**). In the second phase, social novelty preference was tested (preference of novel mouse over familiar mouse). Both groups spent significantly more time exploring the novel mouse compared to the familiar mouse (**Figure 5C**). These data indicate that transient juvenile demyelination results in long-lasting selective impairments of sociability during adulthood.

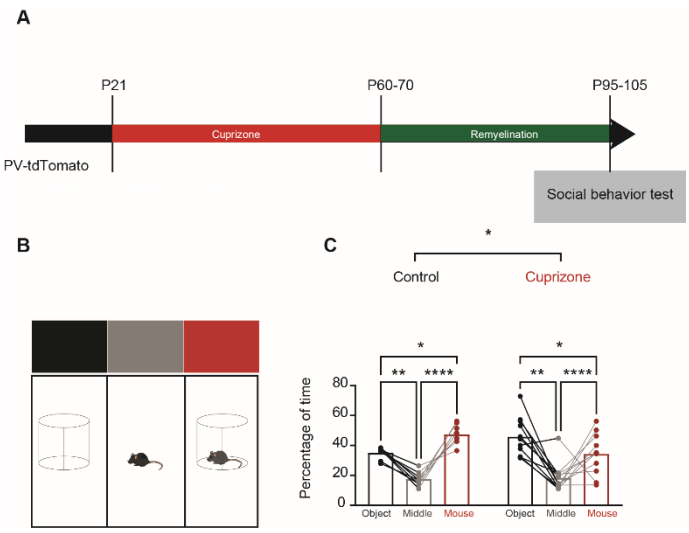

Figure 5. Mice that underwent juvenile demyelination present a significant deficit in social behavior in adulthood. A. Experimental design for the first phase of the three chamber test. **B**. Behavioral results for sociability show that cuprizone mice do not show a social preference while control mice interacted significantly more with the mouse compared to the object (n= 8 control mice and 11 cuprizone mice; two-way repeated measures ANOVA, group x stimulus interaction $F(2,34) = 4.531$, $*p = 0.0180$ followed by post hoc LSD test, $*p < 0.05$, $**p < 0.01$, $***p < 0.001$). **C.** Experimental design for the second phase of the three chamber test. **B**. Behavioral results for social novelty show that both cuprizone mice and control mice showed a preference to interact with the novel mouse compared to the familiar mouse (n= 8 control mice and 11 cuprizone mice; two-way repeated measures ANOVA, group x stimulus interaction $F(2,32) = 0.2412$, $p = 0.7871$ followed by post hoc LSD test, $*p < 0.05$, $**p < 0.01$, $***p < 0.001$).

Adult demyelination alters autaptic transmission but has no effect on PV interneuron maturation and firing abilities

As remyelination was not fully successful in restoring PV interneuron function in the PFC, we hypothesized that the underlying mechanism behind our observations were not solely due to the lack of myelin on PV interneuron, but rather a critical period impairment of PV

developmental maturation. In order to further corroborate this claim, we next examined whether inducing demyelination in adulthood would have different effects on PV interneuron function and self-inhibitory transmission. To this end, cuprizone treatment was initiated at P60 instead of P21 and the duration of the treatment was unchanged. PV interneurons were then examined at P95-105 (**Figure 6A-B**).

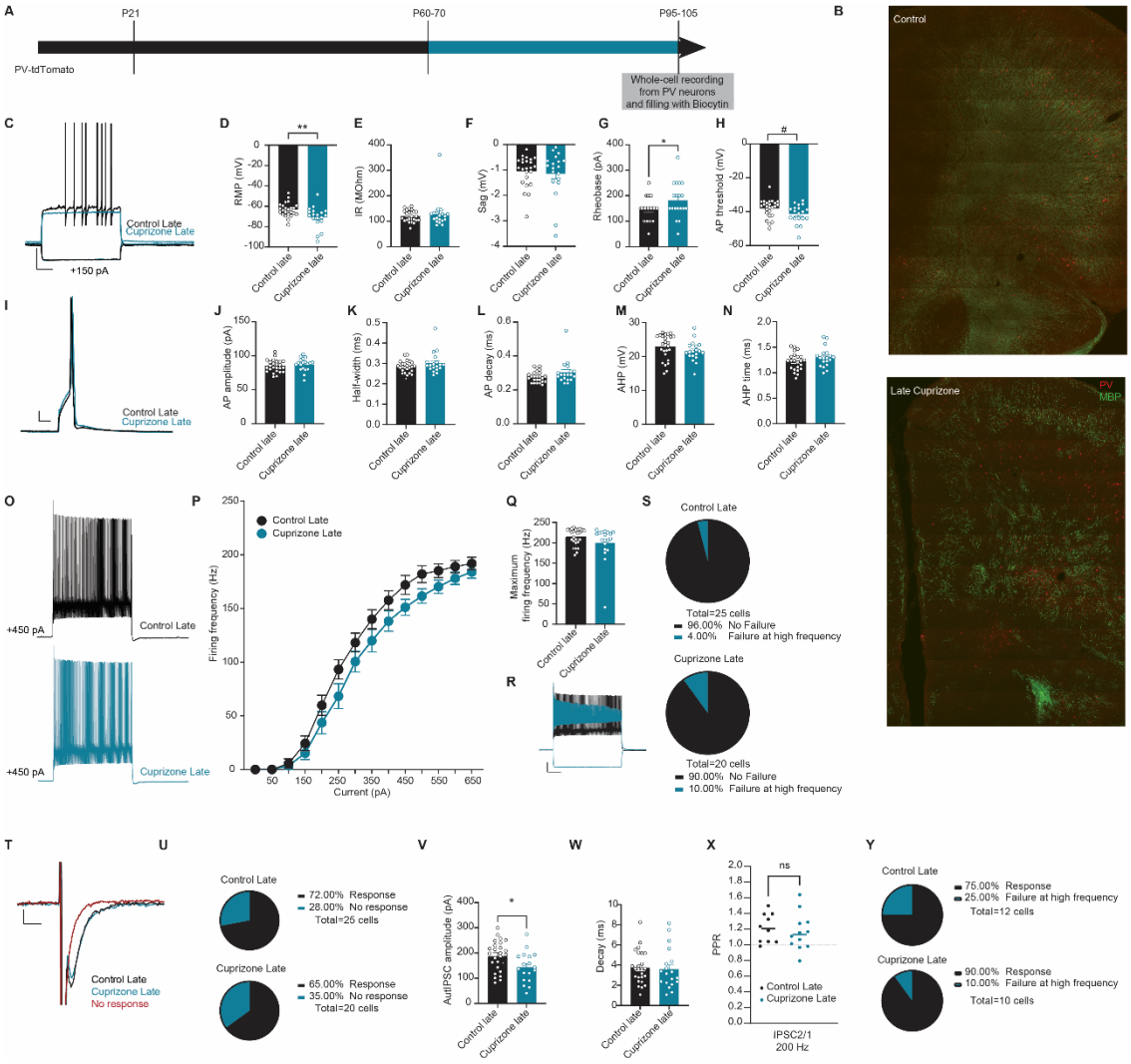

Figure 6. Adult demyelination has no effect on PV interneuron's firing rate or failures in autaptic responses. A. Experimental design for adult demyelination in PV-tdTomato mice. **B**. *Upper panel*. Confocal overview image of PFC in PV-tdTomato animal (tdTomato+, red) overlaid with myelin basic protein (MBP, green). *Lower panel*. Confocal overview image immunolabeled for MBP expression showing the effect of adult demyelination on the PFC region following 6 weeks of 0.2 % cuprizone diet. **C**. Representative traces of voltage responses following a depolarizing step from control (Control Late, black) and adult demyelination (Cuprizone Late, blue) mice illustrating an increased in Rheobase in mice following late cuprizone treatment. **D**-**H**. Summary data showing the averaged (± s.e.m) of the following intrinsic properties: (D) Resting membrane potential (RMP) (*t-test; n= 24,19 cells from 8-6 mice per group, **p = 0.0086*), (E) Input resistance (IR) (*t-test; n= 24,19 cells from 8-6 mice per group, p = 0.5066*), (F) Sag (*t-test; n= 24,19 cells from 8-6 mice per group, p = 0.6607*), (G) Rheobase (*t-test; n= 24,19 cells from 8-6 mice per group, *p = 0.0336*) and (H) Action potential (AP) threshold (*t-test; n= 24,19 cells from 8-6 mice per group, #p = 0.0511*). **I**. A representative trace of a single AP illustrating no difference in AP waveform between late cuprizone (blue) compared to control (black) . **J**-**N**. Summary data showing the averaged (± s.e.m) of the

following AP waveform properties: (J) AP amplitude (*t-test; n= 24,19 cells from 8-6 mice per group, p = 0.3837*), (K) AP half-width (*t-test; n= 24,19 cells from 8-6 mice per group, p = 0.1139*), (L) AP decay (*t-test; n= 24,19 cells from 8-6 mice per group, p = 0.1004*), (M) After-hyperpolarization (AHP) amplitude (*t-test; n= 24,19 cells from 8-6 mice per group, p = 0.2520*) and (N) AHP time (*t-test; n= 24,19 cells from 8-6 mice per group, p = 0.1543*). **O**. Representative traces of voltage responses following +450 pA current injection. **P**. Average action potential (AP) frequency in response to 0-650 pA current steps showing no difference in PV interneuron firing frequency in late cuprizone (blue) mice compared to control (black) mice. (*group x current two-way repeated measures: n = 24/19 cells from 8-6 mice per group: F (13,455)= 1.396, p = 0.1569*). **Q**. Summary data of the maximum firing frequency per group (*t-test; n= 24,19 cells from 8-6 mice per group, p = 0.1581*). **R**. Example trace of a PV interneuron that is unable to maintain high-frequency firing at increased current injection. **S**. Percentage of cells that failed to maintain high frequency firing at > 500 pA was very low after adult demyelination (*Fisher's exact test; p = 0.5772)*. **T.** Representative voltage steps showing an AutIPSC response in control (black) and adult demyelination (blue) groups. The red trace shows a cell that had NO autaptic response. scale: 50 pA, 2 ms. **U**. Adult demyelination mice show no difference in the percentage of cells showing an autaptic response compared to control mice (*Fisher's exact test; p = 0.7488*). **V**. There was a significant decrease in the averaged amplitude of AutIPSCs recorded in mice that underwent adult demyelination (*t-test; n = 26/18 cells from 8-6 mice per group, *p = 0.0194*). **W**. There no difference in the decay of the autaptic post-synaptic currents (*t-test; n = 26/18 cells from 8-6 mice per group, p = 0.7804*). **X**. No difference was detected in the paired-pulse ratio (PPR) between control (black dots) and adult demyelination (blue dots) (*n= 12,10 cells from 8-6 mice per group, p = 0.5780 (IPSC2/1)*). **Y**. There was no difference in the percentage of cells showing a failed autaptic response at 200 Hz remains in the adult demyelination group compared to the control group (Fisher's exact test; *p = 0.5940).

We then assessed PV interneuron properties following adult demyelination (**Figure 6C-N**). PV interneurons showed a significantly more hyperpolarized resting membrane potential and an increased rheobase, indicating a decreased excitability of PV interneurons following adult demyelination (**Figure 6D, G**). Importantly, the input resistance and the sag amplitude were not changed following adult demyelination (**Figure 6E, F**). Furthermore, the AP waveform was not affected by adult demyelination and in turn the firing frequency of PV interneurons from mice that received cuprizone in adulthood was not different from control mice, in contrast to what was observed following juvenile demyelination (**Figure 6I-N, Supplementary Figure 5**). Finally, the maximum firing frequency of PV interneurons following adult demyelination was not decreased compared to control mice (**Figure 6P-Q**). Only 10.0% (2 out of 20) of the cells showed a failure to sustain high firing frequency at high current injections, similarly to 4.0% (1 out of 25) in control mice (**Figure 6R-S**). Together, our data indicates that adult demyelination has no effect on the firing properties of PV interneurons. There was no difference in the percentage of cells showing an autaptic response in mice that received cuprizone treatment in adulthood (65.0%) compared to control mice (72.0%) (**Figure 6T-U**). Interestingly, while juvenile demyelination had no effect on the amplitude of the autaptic response (see Figure 3), adult demyelination caused a significant decrease in the amplitude (**Figure 6V**), but not the decay of the response (**Figure 6W**). Remarkably, adult demyelination had no effect on autaptic plasticity (**Figure 6X-Y**). These data suggest that adult demyelination does not induce a loss of functional autapses, nor does it impair presynaptic GABA release. Rather, the decreased

amplitude of the autaptic response implies a postsynaptic deficit in autaptic transmission following adult demyelination.

Shiverer **PV interneurons have similar properties to juvenile demyelinated PV interneurons, supporting the requirement for myelination in PV interneuron maturation**

Our data thus far point to a clear difference between juvenile demyelination and adult demyelination, highlighting a critical period for PV interneuron maturation and myelination in the PFC. In order to conclusively state that juvenile demyelination impairs the maturation of PV interneurons in the PFC, we made use of *shiverer* mice, harbouring a germline homozygous deletion of MBP. The advantage of this model is that myelination is disrupted from birth. We therefore recoded from *shiverer* and wild-type littermate PV interneurons at P60-75 (**Figure 7A-B**). The data revealed clear similarities between the *shiverer* and the juvenile demyelination groups. First, we examined PV interneuron properties in the PFC of *shiverer* mice. We found considerable similarities between the phenotypes observed in *shiverer* mice compared to mice that underwent juvenile demyelination (**Figure 7C-N**). Specifically, the sag amplitude was significantly increased, while the AP half-width, AP decay time and AHP time were all significantly increased compared to WT mice (**Figure 7E,K,L,N**). Unlike what was observed in adult demyelination, we found no differences in the RMP or rheobase (**Figure 7D,G**). Finally, when we examined the firing properties of PV interneurons, we observed a clear decrease in firing frequency at increased current injections, along with a decrease in the maximum firing frequency in *shiverer* mice (**Figure 7O-S**). This was due to the fact that 37.1% (14 out of 37)of the cells from *shiverer* mice could not sustain high frequency firing (**Figure 7R,S**), a percentage very similar to the juvenile demyelination group of 38.5% (20 out of 52) (see Figure 2P, Q).

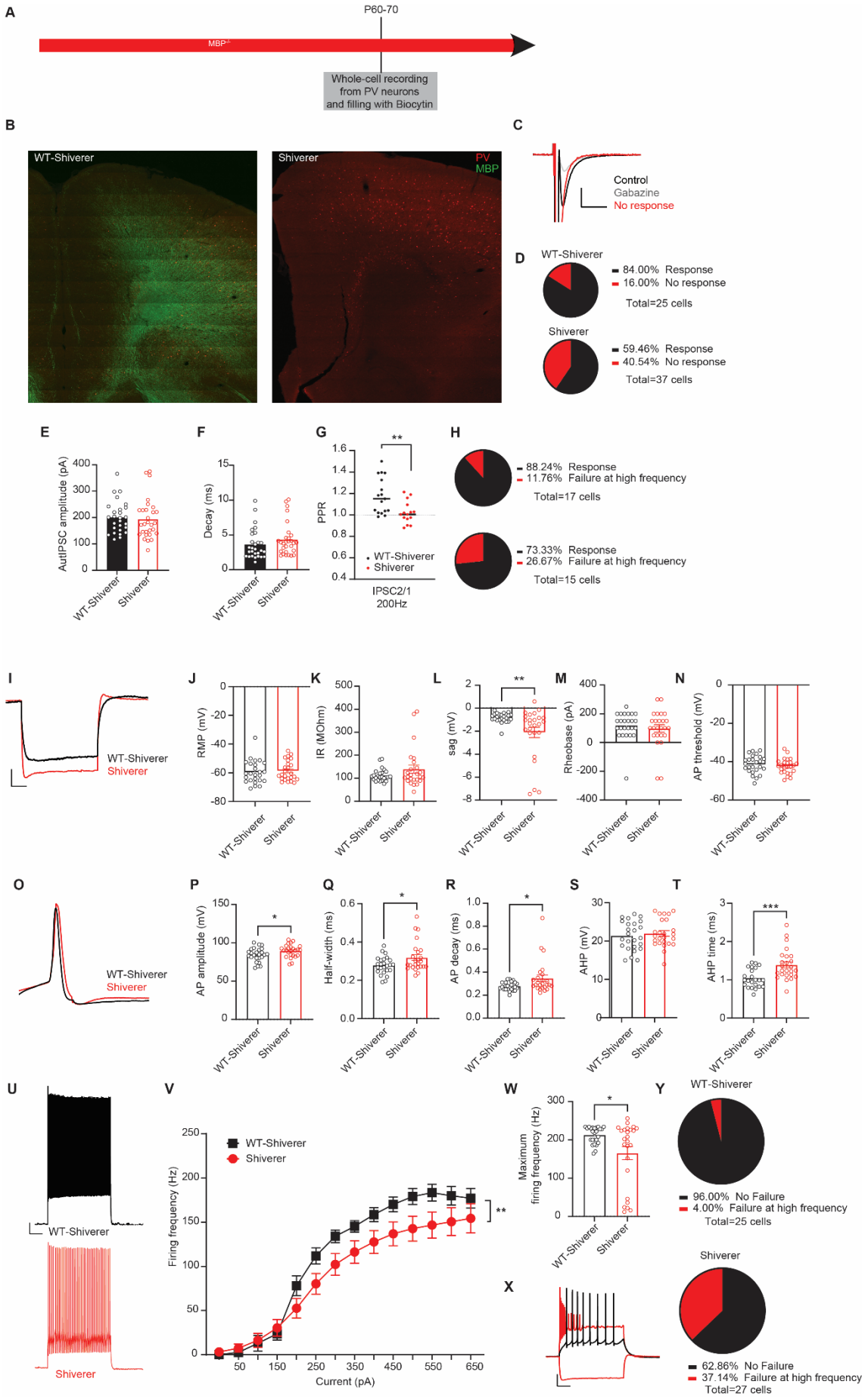
A
P60-70
MBP+/-
Whole-cell recording from PV neurons and filling with Biocytin
B
WT-Shiverer
Shiverer
PV
MBP
C
Control
Gabazine
No response
D
WT-Shiverer
84.00% Response
16.00% No response
Total=25 cells
Shiverer
59.46% Response
40.54% No response
Total=37 cells
E
AutIPSC amplitude (pA)
WT-Shiverer
Shiverer
F
Decay (ms)
G
PPR
IPSC2/1 200Hz
H
88.24% Response
11.76% Failure at high frequency
Total=17 cells
73.33% Response
26.67% Failure at high frequency
Total=15 cells
I
J
RMP (mV)
K
IR (MOhm)
L
sag (mV)
M
Rheobase (pA)
N
AP threshold (mV)
O
P
AP amplitude (mV)
Q
Half-width (ms)
R
AP decay (ms)
S
AHP (mV)
T
AHP time (ms)
U
V
Firing frequency (Hz)
Current (pA)
W
Maximum firing frequency (Hz)
X
Y
96.00% No Failure
4.00% Failure at high frequency
Total=25 cells
62.86% No Failure
37.14% Failure at high frequency
Total=27 cells

Figure 7. PV interneurons from Shiverer mice show many similarities with the ones from mice that underwent juvenile demyelination. A. Experimental design for MBP$^{-/-}$ (Shiverer)-PV-tdTomato mice **B**. *Left.* Confocal overview image of PFC in control PV-tdTomato animal (tdTomato+, red) overlaid with myelin basic protein (MBP, green). *Right.* Confocal overview image immunolabeled for MBP expression showing the absence of myelination in the PFC of Shiverer mice. **C**. Representative traces of voltage responses following a hyperpolarizing step from control (black) and Shiverer (light red) mice illustrating an increased sag in mice lacking MBP from birth. **D**-**H**. Summary data showing the averaged (± s.e.m) of the following intrinsic properties: (D) Resting membrane potential (RMP) (*t-test; n = 25/25 cells from 9 mice per group, p = 0.6752*), (E) Input resistance (IR) (*t-test; n = 25/25 cells from 9 mice per group, p = 0.1407*), (F) Sag (*t-test; n = 25/25 cells from 9 mice per group, **p = 0.0072*), (G) Rheobase (*t-test; n = 25/25 cells from 9 mice per group, p = 0.5406*) and (H) Action potential (AP) threshold (*t-test; n = 25/25 cells from 9 mice per group, p = 0.4461*). **I**. A representative trace of a single AP illustrating a wider and slower AP in Shiverer mice (light red) compared to control (black) . **J-N**. Summary data showing the averaged (± s.e.m) of the following AP waveform properties: (J) AP amplitude (*t-test; n = 25/25 cells from 9 mice per group, *p = 0.0405*), (K) AP half-width (*t-test; n = 25/25 cells from 9 mice per group, *p = 0.0278*), (L) AP decay (*t-test; n = 25/25 cells from 9 mice per group, *p = 0.0258*), (M) After-hyperpolarization (AHP) amplitude (*t-test; n = 25/25 cells from 9 mice per group, p = 0.5188*) and (N) AHP time (*t-test; n = 25/25 cells from 9 mice per group, ***p = 0.0007*). **O**. Representative traces of voltage responses following +450 pA current injection. **P**. Average action potential (AP) frequency in response to 0-650 pA current steps illustrating a significant decrease in PV interneuron firing frequency in Shiverer mice (*group x current two-way repeated measures: n = 25/25 cells from 9 mice per group: F(13,624)= 2.303, **p < 0.0056*). **Q**. Summary data of the maximum firing frequency per group (*t-test; n = 25/25 cells from 9 mice per group, *p = 0.0109).* **R**. Example trace of a PV interneuron that is unable to maintain high-frequency firing at increased current injection. **S**. Percentage of cells that failed to maintain high frequency firing at > 500 pA in both groups reveals a clear increase in Shiverer mice (*Fisher's exact test; **p = 0.0041*). **T**. Representative voltage steps showing an AutIPSC response in blackand no response in red. The red trace shows a cell that had NO autaptic response. Scale:100 pA, 5ms. **U**. Shiverer mice show a clear decrease in the percentage of cells showing an autaptic response compared to control mice (*Fisher's exact test; p = 0.0516*). **V**-**W**. There was no difference between groups in the amplitude (V) or decay (W) of the autaptic post-synaptic currents in cells that had autapses in the Shiverer mice (light red) compared to the control mice (black) (*t-test; n = 27/29 cells from 9 mice per group, p = 0.7167 (V) and p = 0.2377 (W)*). **X**. Short-term plasticity of autaptic responses at 200 Hz is impaired in shiverer mice (light red) compared to control (black) mice (*n=17/15 cells from 9 mice per group,**p = 0.0041 (IPSC2/1)*). **Y**. There was no significant difference in the percentage of cells showing a failed autaptic response at 200 Hz remains in the Shiverer group compared to the control group (Fisher's exact test; p = 0.3828).

Next, we recorded autaptic responses from PV interneurons from both groups. 59.5% of PV interneurons from *shiverer* mice showed no autaptic responses compared to 20.0% in their wild-type littermates (**Figure 7T,U**). The amplitude and decay of the autaptic responses were not affected (**Figure 7V,W**). On the other hand, short-term plasticity at 200 Hz was significantly impaired (**Figure 7X, Y**).

PV interneurons show a significant decrease in Kv3 currents and Kv3 expression following juvenile demyelination

Finally, we sought to unravel the mechanism by which juvenile demyelination could be impairing PV interneurons firing at high frequency. The ability of PV interneurons to sustain high frequency firing results from their very fast AP properties endowed by a prominent expression of Kv3 channels[26]. In fact, previous studies have shown an upregulation of K+ channel subunits of the Kv3 subfamily during the second and third postnatal week that drives these specific features of fast-spiking PV interneurons[1,23]. Therefore, we aimed to examine whether the immature phenotype displayed by PV interneurons following juvenile demyelination could be explained by changes in K+ currents in these cells. To that end, we performed voltage-clamp recordings from PFC PV interneurons following cuprizone treatment (**Figure 8**). The amplitude of the K+ currents from +10 mV to +60 mV was significantly lower in PV interneurons following juvenile demyelination (**Figure 8A-B**). A two-way ANOVA test revealed that both demyelination and the voltage step had a significant effect on the amplitude of the resulting K+ currents (**Figure 8B**). To verify that these changes in K+ currents were at least partly due to changes in Kv3 channel activity, we performed the same voltage-clamp recordings in the presence of TEA (1 mM), which results in a relatively selective block of Kv3 potassium channel[24] (**Figure 8C**). The data confirmed a decrease in TEA-sensitive currents in the cuprizone group, with a clear interaction effect (group x voltage) (**Figure 8D**).

Next, we used immunolabeling against Kv3.1b channels to quantify Kv3 channel expression in PV interneurons from the cuprizone group (**Figure 8E**). We observed a clear reduction of Kv3 immunofluorescence along PV interneurons of the PFC in mice that underwent juvenile demyelination compared to controls, while PV expression and cell density were unaltered (**Figure 8F-J, Figure 1H,I**). Together, our results uncover that juvenile demyelination leads to a decrease in Kv3 channel expression and activity within PV interneurons of the PFC.

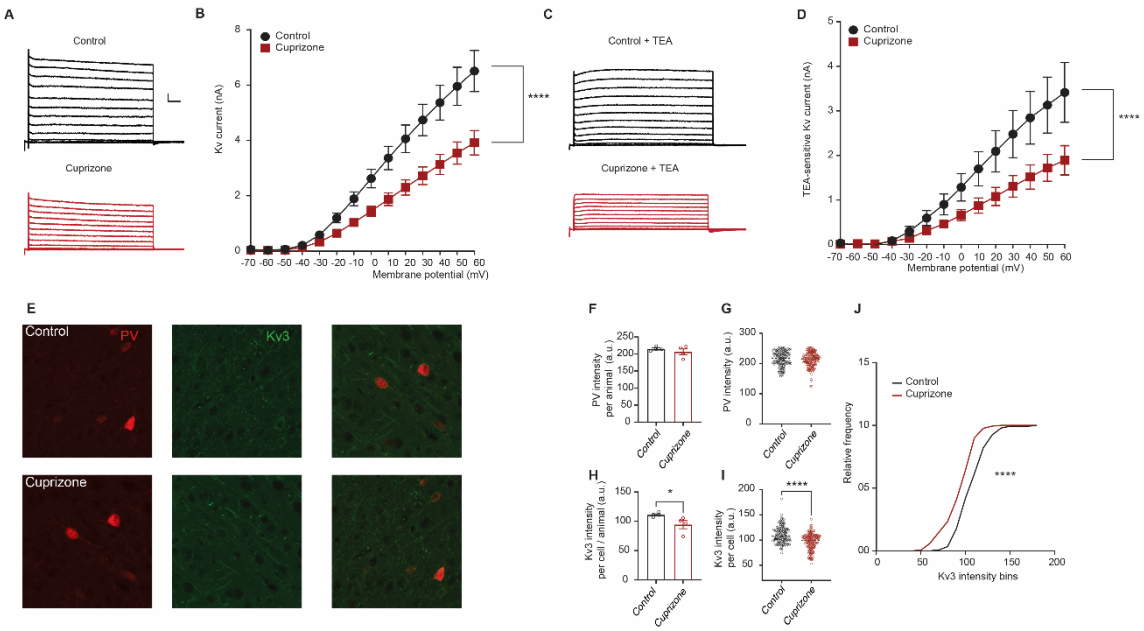

Figure 8. Juvenile demyelination leads to a substantial decrease in potassium currents in PV interneurons of the PFC. A. Representative traces of potassium currents evoked with 10 mV potential steps from -70mV to +60 mV in PFC PV interneurons from control (black) and cuprizone (red) mice. Scale: 500 pA, 100 ms. **B**. I–V curves showing a significant decrease in Kv amplitude in PV interneurons from mice that underwent juvenile demyelination. (*group x voltage two-way repeated measures: n = 12,18 cells from 5 mice per group: $F(13,364)= 10.45$, $p < 0.0001$).* **C**. Representative traces of TEA-sensitive potassium currents (1mM). **D**. TEA-sensitive currents were specifically decreased in PV interneurons from mice that received cuprizone treatment compared to control mice (*group x voltage two-way repeated measures: n = 10,14 cells from 5 mice per group: $F(13,286)= 5.082$, $p < 0.0001$*). **E**. Representative images of double immunostaining of PV interneurons (red) and Kv3.1b (green) in the PFC in control and cuprizone mice. **F**-**G**. PV intensity was not altered following juvenile demyelination (*t-test of (F); n = 4 mice per group, $p = 0.3888$; t-test of (G); n = 145/170 cells from 4 mice per group, $p = 0.3067$*). **H**-**J**. Kv3.1b intensity was significantly decreased in PV interneurons from cuprizone mice (red) compared to control mice (black) (*t-test of (H); n = 4 mice per group, $p = 0.0286$; t-test of (I); n = 145/170 cells from 4 mice per group, $p < 0.0001$, Kolmogorov-Smirnov test of (J); $p < 0.0001$*).

Modulation of Kv3 channels results in a partial rescue of PV interneuron properties in cuprizone mice

In order to test whether decreased Kv3 activity underlies the observed phenotypes reported in PV interneurons after juvenile demyelination, we used AUT00201, a positive modulator of Kv3 potassium currents[25], to evaluate whether we can rescue PV interneuron properties in the early cuprizone mice. To that end, we measured intrinsic properties of PV interneurons at baseline and following 5 min of bath application of AUT00201 (1uM) (**Figure 9**). We found that AUT00201 decreased the rheobase of PV interneurons from early cuprizone mice but not control mice (**Figure 9A**). Importantly, AUT00201 was able to fully rescue AP half-width in PV interneurons of early cuprizone mice while having no effect in control mice (**Figure 9B**). Intriguingly, AUT00201 decreased the firing threshold of PV interneurons in both conditions while the remaining properties of PV interneurons were unaltered (**Supplementary Figure 6**).

As AUT00201 induced a clear rescue of AP half-width in early cuprizone mice, we then wondered if the firing rate of PV interneurons could be rescued by bath application of AUT00201 (1uM). However, when we looked at the firing frequency curves, we did not see any overall significant improvement (**Supplementary Figure 6F**). After a close examination of the effect on AUT00201 on individual cell firing patterns, we found that it was able to improve firing in 61.5 % (8 out of 13) of PV interneurons from early cuprizone mice while having no effect in 23.0% of cells (3 out of 13) and impairing the firing in 15.4% of the cells (2 out of 13) (**Figure 9C, Supplementary Figure 7**). Conversely, in control cells, AUT00201(1uM) increased PV interneuron firing in only 8.3% of the cells (1 out of 12), whereas it had no effect on the firing properties in 58.3% of the cells (7 out of 12). AUT00201 even induced an impairment in firing at high current injections in 33.3% of cells from control mice (4 out of 12) (**Figure 9C-D**). Analysis of only the positively affected cells in the early cuprizone group revealed an increase in the firing frequency of PV interneurons after AUT00201 application (**Figure 9E**). Taken

together, these data imply that juvenile demyelination impairs the maturation of PV interneurons by affecting Kv3 channel activity and expression. Interestingly, bath application of the Kv3 modulator AUT00201 (1uM) had no effect on PV properties in the late cuprizone group (**Supplementary Figure 8**).

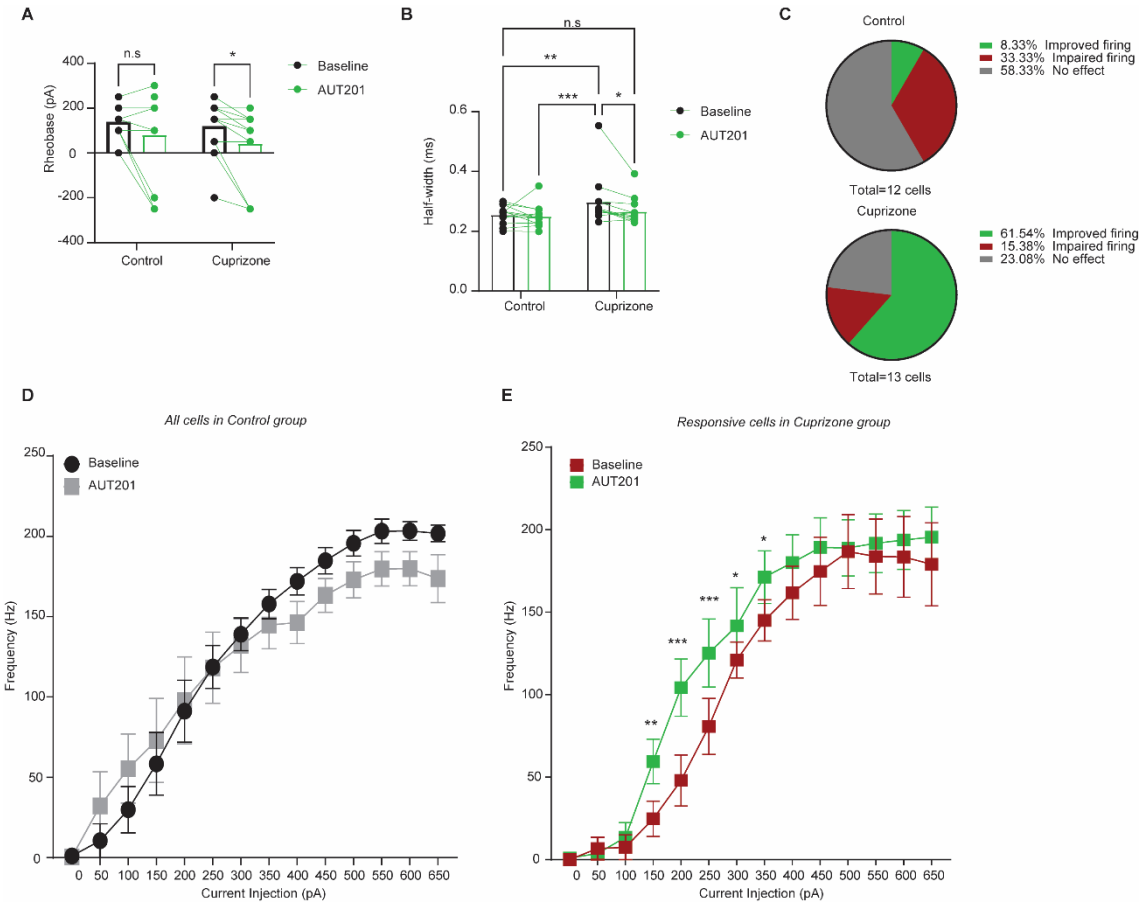

Figure 9. AUT00201 (1uM) can rescue AP width in cuprizone mice. A. Bath application of AUT00201 1um decreased the rheobase of PV interneurons from cuprizone mice but not control mice (*group x AUT00201 two-way repeated measures: n = 12,13 cells from 4 mice per group: F(1,12)= 0.1816, p = 0.6775; AUT00201 effect: F(1,12)= 7.122, *p = 0.0205. Post-hoc LSD test: *p < 0.05, n.s. p = 0.0957*). **B**. AUT00201 restores AP half-width in PV interneurons from cuprizone mice, while having no effect on cells from control mice (*group x AUT00201 two-way repeated measures: n = 12,13 cells from 4 mice per group: F(1,12)= 2.774, p = 0.1217; AUT00201 effect: F(1,12)= 5.685, *p = 0.0345. Post-hoc LSD test: *p < 0.05, **p < 0.01, ***p < 0.001, n.s. p = 0.3148*). **C**. Pie charts reflecting the effect of AUT00201 on PV interneurons firing frequency in control (upper) and cuprizone (lower panel) mice. **D**. Average action potential (AP) frequency in response to 0-650 pA current steps suggesting an impairment at high-frequencies in control cells after bath application of AUT00201 (1uM) (grey) (*group x current two-way repeated measures: n = 13 cells from 4 mice: p = 0.1369).* **E**. In the responsive cells from cuprizone mice (red) a significant increase in PV interneuron firing frequency at lower current steps (green) was observed (*group x current two-way repeated measures: n = 8 cells from 4 mice: p = 0.05287; AUT00201 effect: F(1,60)= 5.050, *p=0.0457. Post-hoc LSD test: *p < 0.05, **p < 0.01, ***p < 0.001*).

Discussion

Autapses play a role in high frequency firing of PV interneurons

Previous studies have demonstrated that fast-spiking interneurons undeniably exhibit autapses, which are synaptic contacts between the cell's own soma or dendrite and its own axon[3,18-20,26]. While there is still a lot unknown about the role of these autapses, it has been proposed that they play an important role in PV interneuron's specific temporal control of microcircuits. Specifically, autaptic neurotransmission has been put forward as a particular form of cortical disinhibition that adds to PV interneuron's role in controlling network oscillations[18,19]. On average, 70 to 80% of PV interneurons have autapses, while non-fast-spiking interneurons do not display such features[19-21,26]. Autapses in PV interneurons release GABA with high probability, and plasticity at autaptic sites is similar to synaptic plasticity at non-autaptic inhibitory postsynaptic sites[18,20,21,26]. Interestingly, a recent study found autaptic neurotransmission to be stronger that synaptic transmission in some PV interneurons and they estimated that autaptic transmission accounted for approximately 40% of the global inhibition that PV interneurons received[18].

Where are these autapses located? Just as PV interneurons synapse onto the perisomatic region of their connected partners, autapses are present exclusively in close vicinity (circa 50 µm) of the soma of PV interneurons[3,20]. Micheva and colleagues used high resolution array tomography to confirm the presence of these autapses structurally in PV interneurons and they reported that the number of autapses is stable during development until adulthood, with an average of 6 ± 3 autapses per cell, which is in agreement with previous reports[3,19,20,26]. A recent study by Deleuze and colleague was the first to validate a potential role of autaptic connections in PV interneuron's role in controlling network oscillations. They uncovered that AP-evoked autaptic release modulates the coupling of PV-cell spikes with γ-oscillations by regulating spike AHP and interspike intervals[18]. In the current study, we aimed to explore whether autapses might play a role in PV interneuron's ability to fire at high frequency, which in turn has been demonstrated to be of importance for network oscillations and higher cognitive processing[18,19]. We show that PV interneurons without autapses are more excitable, displaying a lower rheobase and a change in the AP's AHP. Interestingly, these cells had higher firing frequencies at low current injections, yet they had a significantly decreased maximum firing rate. These data suggest that autapses contribute to PV interneuron's ability to fire at high frequency by controlling the excitability and the timing of PV interneurons spiking activity, as postulated in previous studies.

Myelination of PFC PV interneurons during adolescence is crucial for their structural maturation

Recent work has been focused on exploring the function of myelination in local interneurons, as opposed to the more classical approach of studying myelination in long projection neurons[4,5]. Several of these studies have highlighted the importance of adult PV interneuron myelination in proper PV interneuron function, such as inhibitory control of local oscillations,

experience-dependent plasticity or AP conduction velocity increase along PV axons[6,8,27]. Yet, little is known on whether PV interneuron myelination is important for their own development and maturation. Few studies have demonstrated that disrupting early glia-PV interneuron interaction can have an effect on PV interneuron myelination and subsequent PV interneuron maturation and function[7,9]. Moreover, studies examining mouse model of neuropsychiatric disorders have uncovered myelin deficits in PV interneurons[10,28]. Given the implications of PFC development in many neuropsychiatric disorders, along with a clear role of PV interneuron dysfunction in such disorders, adding to it the various reports of myelin deficits in patients with neuropsychiatric disorders[10], we aimed to investigate whether an early disruption of PV interneuron myelination, during the critical period of PFC development, can lead to an impairment in their maturation and development. Many studies report that the critical period for PFC maturation expands from P21 to P35[14,22,29,30]. We used the cuprizone model starting at P21 in order to achieve juvenile demyelination in PV-tdTomato mice. Our data revealed that juvenile demyelination can lead to clear alterations in PV interneuron morphology in adulthood. Specifically, we found a decrease in the total axonal length, as well as the total number of axonal branches in PV interneurons from mice that underwent juvenile demyelination. The axons of PV interneurons were reported to be quite dynamic during the second and third postnatal week, at a time where myelination is starting to peak[3,31]. Taken together, our results indicate that myelination is crucial for the proper development of PV interneuron axons during this time window.

Myelination of PFC PV interneurons during adolescence is important for self-inhibitory transmission

What happens to autapses following juvenile demyelination and this subsequent aberrant development of PV interneurons? Our data revealed a significant decrease in the number of PV interneurons that have autaptic responses after juvenile demyelination, but not after adult demyelination. When examining the filled and reconstructed neurons, we found that around 25% of PV interneurons from the juvenile demyelination group had structural autapses but showed no autaptic responses, indicating that the loss of myelin during adolescence had led to some failures in autaptic neurotransmission. Moreover, around 30% of the cells had no autapses at all, compared to around 11% in controls, pointing to a complete loss of autapses in some PV interneurons after juvenile demyelination. Yet, more than 45% of PV interneurons in that group still had functional autapses, with the amplitude of the responses also largely unaffected. Therefore, we next investigated whether plasticity at autaptic sites was impaired as a result of juvenile demyelination. Our data uncovered an impairment in short-term plasticity at autaptic sites at 50 Hz and 200 Hz but not at 20 Hz, indicating that myelination during adolescence is required for adult synaptic plasticity, especially at high frequencies. Results in *shiverer* PV interneurons confirmed these data. Conversely, in mice that underwent adult

demyelination, short-term plasticity at autaptic sites was not affected, although, the amplitude of the inhibitory autaptic response was decreased. This is likely due to a deficit in inhibitory synapse stabilization and maintenance caused by the loss of myelin, as exposed by previous studies[8]. Together, our data suggest that juvenile demyelination can cause a total loss of functional autapses in PV interneurons of the PFC and impair presynaptic release at autaptic sites. It remains to be investigated whether the deficits in short-term plasticity recorded in PV interneurons from mice that underwent juvenile demyelination are due to failures in AP-triggered GABA release or failures of AP propagation along demyelinated axons.

Myelination of PFC PV interneurons during adolescence is critical for PV interneuron electrophysiological maturation

Our data so far has demonstrated that juvenile demyelination can cause an extensive impairment in the development of PV interneuron axons, can induce a loss of functional autapses and can undermine synaptic plasticity at autaptic sites. Do these have an effect on PV interneuron intrinsic properties and electrophysiological development? Our data revealed that PV interneurons in the PFC of mice that underwent juvenile demyelination show clear maturation deficits in their intrinsic properties. Specifically, we observed an increase in the input resistance and sag amplitude, an increase in AP width and a substantial decrease in the firing frequency, especially at high frequencies, all reminiscent of immature PV interneurons[1,23]. Importantly, around 40 % of the cells could not sustain their firing at high frequency and the maximum firing rate was drastically decreased. Similar observations were made in the shiverer model, indicating that the lack of myelin during this critical period of development had significant impact on the electrophysiological maturation of these cells. Indeed, in mice that underwent adult demyelination, while PV interneurons were found less excitable, which is in agreement with previous studies[8], there were no changes observed in any of these parameters and the maximum firing rate of these cells was not affected. It is also interesting to note that while juvenile demyelination led to a decrease in the percentage of the PV interneurons with autaptic responses in the S1 area, no impairment in the firing frequency was observed in this region, highlighting a regional difference in the importance of myelination to PV interneuron development.

Early cuprizone treatment might be impairing necessary communication between glial cells and PV interneurons in the PFC

There have been only a few studies that explored the role of myelination on PV interneuron development and maturation. Specifically, these studies used mouse models where the communication between OPCs and neurons is disrupted from birth[7,9]. In these models, PV interneurons showed impaired maturation which was manifested in some case by a decreased firing rate of these neurons. Given the similarities that we detect between the mice that underwent juvenile demyelination and the shiverer mice, we propose that our early

intervention is impairing the necessary communication between PV interneurons in the PFC and their respective OPC partners. In fact, when mice received cuprizone in adulthood, PV interneurons had no impairments in their firing rate. Moreover, mice that underwent juvenile demyelination had long-lasting impairment in their maturation, which persisted even 5-6 weeks after remyelination. Together, these data indicate that myelination alone is not the determining factor in the observed impairments in PV interneuron properties. It is rather myelination during this critical period (P21-P50) that is crucial for PV interneuron development.

Remyelination after juvenile demyelination is unable to fully rescue PV interneuron function and PFC-dependent social behavior

Remyelination studies have revealed that in only 4 weeks after prolonged cuprizone treatment, full remyelination can occur[32–35]. We hence investigated whether remyelination could restore PV interneuron propertied and autaptic neurotransmission following juvenile demyelination. Our data showed that while many of the membrane properties were rescued by remyelination, PV interneuron's firing rate was still decreased after remyelination and more than 25% of the cells could not sustain their firing rate at high frequencies. Interestingly, autaptic responses at high frequency were also still impaired. This suggests that restoring myelin in the PFC might have reinstated some channel properties in PV interneurons, yet the ability of PV interneurons to fire at high frequency was not fully restored. We propose that the loss of myelin during this critical period of PFC development constrict any full rescue of PV interneuron properties as many previous works have confirmed that this is a sensitive period for PFC development and any intervention during this vulnerable period could have long-lasting effects. It is noteworthy that remyelination rescued all PV interneuron properties in S1.

Studies have showed that insults to PFC during this critical period can have long-lasting detrimental effects on social behavior. Moreover, impairments in PV interneuron function during this juvenile period lead to deficits in adult social behavior. Accordingly, we uncovered that mice which underwent juvenile demyelination followed by a period of remyelination, a timepoint where we showed that PV interneurons function was not yet fully restored in the PFC, showed clear social deficits. This data implies that juvenile demyelination can lead to long-last impairment in PV interneuron function which could explain social impairments in adulthood.

Kv3 is crucial for PV maturation and myelination

PV interneuron electrophysiological maturation has been closely linked to the development of distinct ion channels that allow for their unique ability to fire at high frequencies. Specifically, Kv3 channels have been shown to double its expression level from P18 to P30[1]. While a decrease in Kv3 channel would not explain the increased input resistance and sag in PV interneurons following juvenile demyelination, it could explain the increased AP width and firing frequency. Therefore, we next explored whether a loss of myelin during adolescence

could be affecting Kv3 expression and activity levels in PV interneurons of the PFC. Previous studies have demonstrated that myelination causes alterations in Na+ and K+ channels in pyramidal neurons[36]. Our results confirmed a clear decrease in Kv3.1 expression level, using immunohistochemistry, and activity level , using voltage-clamp recordings from PV interneurons of the PFC in mice that underwent juvenile demyelination. We next tested whether AUT00201, a positive modulator of Kv3 K+ currents, could restore Kv3 currents in PV interneurons from mice that underwent juvenile demyelination. Remarkably, bath application of AUT00201 could fully rescue the AP width deficit. This is exciting as it points to the potential for therapeutic benefit in neurodevelopmental disorders where PV interneuron function, including reduced Kv3 channel expression occurs[37]. Yet, the impaired firing was only improved in around 60% of the tested cells from the cuprizone mice. This indicates that, while Kv3 activation can restore AP waveforms in these cells, the loss of Kv3 expression due to juvenile demyelination makes it difficult for such an intervention to fully rescue PV properties in our model.

Unsurprisingly, our data points out to other channels that might also be affected by the early cuprizone treatment. The changes in the sag that was reported in both the early cuprizone group and the shiverer mice hint to alteration in HCN channels. HCN channels, which were found to be exclusively localized on axons in PV interneurons, play a critical role in enhancing AP initiation during sustained high-frequency firing and in increasing the velocity by which APs propagate in PV interneuron axons[38]. Further work examining whether juvenile demyelination is altering HCN channels in PV interneurons would be essential for future studies. Another interesting subtype of K+ channel that might be affected in our model is the TASK channel subtype. TASK-1 and -3 levels were reported to be increased at P18 compared with P10 and PV interneurons from TASK-1/3 double knock-out mice have an increased input resistance, wider AP and a decreased firing rate[39]. Future work should be focused on unravelling the specific channels that are underlying the deficits we report in PV interneurons following juvenile demyelination.

Relevance for human disorders

The development of PFC circuits is known to extend beyond the juvenile developmental period[15,17]. It is characterized by an essential maturation of inhibitory networks and the establishment of excitatory/inhibitory balance, which in turn give rise to various brain oscillations involved in higher cognitive functions[17,40]. PV interneuron development follows a prolonged period of maturation that also extends into adolescence[1,10,23]. While many studies have attributed an impairment in PFC development and PV interneuron maturation to many neuropsychiatric disorders[12], little is known about whether there is a link between myelination and PV interneuron development in the PFC. Makinodan and colleagues were the first to unravel a critical period for oligodendrocyte maturation and myelination for PFC-dependent

social behaviour[22]. They showed that social isolation of mice between P21 and P35 can have long lasting effects on PFC myelination, where mice that underwent social isolation in this period showed less myelin expression in the PFC compared to mice that were socially isolated after P35 and control mice. Furthermore, mice in which myelination was impaired because of loss of ErbB3 signalling (starting P21) showed similar social behaviour deficits to the ones elicited by social isolation during the critical period, confirming that myelination of the PFC during this period is necessary for normal social behaviour in the adult. Interestingly, another study uncovered that demyelination in juvenile mice, but not in adulthood, can lead to long-lasting impairments in social interaction in mice[30]. Finally, it has been shown that social isolation during this critical period (P21-35) can have significant effects on PV interneuron activity in the PFC, specifically PV interneurons from mice that underwent social isolation during this period had a decreased firing rate. Taken together, we propose that our data unravels an important link between PV interneuron myelination and their development in the PFC during this critical period, which offers key insights into the mechanisms underlying the pathophysiology and potential therapies for neurodevelopmental disorders.

Materials and Methods

All experiments were conducted under the approval of the Dutch Ethical Committee and in accordance with the Institutional Animal Care and Use Committee (IACUC) guidelines. The Pv-tdTomato [Tg(Pvalb-tdTomato)15Gfng] line was used as well as the Shiverer [B6;C3Fe.SWV-Mbpshi /J (Shiv) (Chernoff 1981; www.jax.org/strain/001428)] line that was crossed with the Pv-tdTomato line .

For cuprizone treatment, mice received 0.2% (w/w) cuprizone (Bis(cyclohexanone)oxaldihydrazone (C9012, Merck) added to grinded powder food or to food pellets (Envigo). For the juvenile demyelination group, mice received fresh cuprizone food starting at P21 for a period of 6-7 weeks while control mice received control food, both ad libitum. For the adult demyelination group, mice received either cuprizone food (cuprizone group) or normal chow food (control group) starting P60 for a period of 6-7 weeks. The average maximum weight loss during cuprizone treatment was around 15 % in the Adult cuprizone group and around 7 % in the juvenile demyelination group. All. Mice from both sexes were used for these experiments. All mice were maintained on a regular 12 h light/dark cycle at 22 °C (±2 °C) with access to food and water *ad libitum*.

Slice preparation and electrophysiology

Mice were quickly anaesthetised with isofluorane and decapitated. Brains were rapidly dissected and placed in ice-cold partial sucrose solution containing (in mM): sucrose 70, NaCl 70, $NaHCO_3$ 25, KCl 2.5, NaH_2PO_4 1.25, $CaCl_2$ 1, $MgSO_4$ 5, sodium ascorbate 1, sodium pyruvate 3 and D(+)-glucose 25 (carboxygenated with 5% CO_2/95% O_2). 300 µm thick coronal

slices from the prefrontal and somatosensory cortices were obtained with a vibrating slicer (Microm VT1200 S, Leica) and incubated for at least 20 min at 38 °C in holding artificial cerebro-spicnal fluid (ACSF) containing (in mM): 127 NaCl, 25 $NaHCO_3$, 25 D(+)-glucose, 2.5 KCl, 1.25 NaH_2PO_4, 1.5 $MgSO_4$, 1.6 $CaCl_2$, 3 sodium pyruvate, 1 sodium ascorbate and 1 $MgCl_2$ (carboxygenated with 5% CO_2/95% O_2). Next, slices were transferred into the recording chamber where they were continuously perfused with recording ACSF (in mM): 127 NaCl, 25 $NaHCO_3$, 25 D-glucose, 2.5 KCl, 1.25 NaH_2PO_4, 1.5 $MgSO_4$ and 1.6 $CaCl_2$. We used an upright microscope (BX51WI, Olympus Nederland) equipped with oblique illumination optics (WI-OBCD; numerical aperture 0.8) and a 40x water-immersion objective to visualise the tissue. Images were collected with a CCD camera (CoolSMAP EZ, Photometrics) regulated by Prairie View Imaging software (Bruker). PV-positive interneurons neurons were visualized using a DsRed filter (Semrock, Rochester, NY, USA).

Electrophysiological recordings were acquired using HEKA EPC10 quattro amplifiers and Patchmaster software at 33°C. Borosilicate glass patch pipettes (Harvard Apparatus) were pulled with 3-6 MΩ series resistance and filled with with a high [Cl−] intracellular solution containing (in mM) 70 K-gluconate ,70 KCl, 10 HEPES, 1 EGTA, 2 MgCl2, 2 MgATP, and 0.3 NaGTP with 5 mg/mL biocytin; pH 7.2 adjusted with KOH; 285 mOsm. The estimated E_{Cl} was around –16 mV based on the Nernst equation. All recorded cells had a series resistance below 20 MΩ with correct bridge balance and capacitance fully compensated. AMPA-mediated currents were blocked using DNQX (10 μM). Gabazine (10 μM) was also used by bath perfusion to block GABAARs.

Whole-cell current-clamp and voltage-clamp recordings were performed on PV interneurons in layers 2-3 in both the PFC and S1. AutIPSC recordings were measured as described previously; PV interneurons were clamped at -80 mV. Brief depolarizing voltage steps (0.2-0.6 ms, from -80mV to 0 mV) were injected in PV interneurons in order to induce a GABAergic response that was abolished by Gabazine. The amplitude and decay of the response were averaged over 8 trials. Short-term plasticity at autaptic sites was examined by evoking a train of 5 events at 20 and 50 Hz, or a train of 100 events at 200 Hz. Asynchronous release of GABA at autaptic site was induced as previously reported; PV interneurons were recorded in voltage-clamp mode and an increase in spontaneous inhibitory events was the result of trains of high-frequency stimulation (200 Hz, 100 AP), completely abolished by gabazine. For Kv current recordings, holding potential was -70 mV and voltage steps from -70 mV to +60 mV (in 10 mV increments) were recorded to extract high voltage activated potassium currents. Tetrodotoxin (1uM) was used to suppress sodium- activated channels. TEA (1mM) was applied to the bath following baseline recordings. The resulting voltage currents were obtained by subtraction of baseline from TEA-sensitive currents. Leak currents were removed online.

Intrinsic passive and active membrane properties were recorded in current-clamp mode, both at resting membrane potential and at -70 mV, by injecting 500-ms of increasing current stimuli from -300 pA to +650 pA, at intervals of 50 pA. Input resistance was calculated from hyperpolarizing current injections. Sag was obtained from the average voltage difference between the lowest voltage response and the steady-state response at -300 pA to -100 pA. Action potential (AP) waveform characteristics were derived from the first action potential. AP amplitude was defined as the voltage difference between peak voltage and the threshold. AP half-width was measured at half of the peak amplitude. AP decay time was quantified as duration from 100% to 10% of the peak amplitude. The fast after-hyperpolarizing potential (AHP) amplitude was measured as the peak hyperpolarizing voltage from AP threshold after the decay of the AP. AP frequency was determined from the number of APs in response to a square-wave current pulse of 500 ms duration. Data analysis was conducted using a custom-designed script in Igor Pro-9.0 (Wavemetrics).

AUT 201 compound

AUT00201 (Autifony Therapeutics) is a small molecule modulator of Kv3.1 and Kv3.2 channels. AUT00201 (10 mM stock solution) was dissolved in DMSO (0.1%), and the final concentration used in the recording chamber was 1 uM.

Immunohistochemistry

Patch-clamp recorded PV interneurons were filled with 5mg/mL biocytin during whole-cell recordings and then fixed with 4% (PFA) overnight and stored in PBS at 4°C. Slices were then stained with streptavidin-Cy3 secondary antibody (1:300; Invitrogen), 0.4% Triton X-100 and 2% NHS in PBS during 2 h. Slices were mounted and coverslipped with Mowiol (Sigma). For staining performed on free-floating brain sections, mice were anesthetised by intraperitoneal injection of pentobarbital, and transcardially perfused with saline followed by 4% paraformaldehyde (PFA). Brains were dissected and postfixed in 4% PFA for 2 h at room temperature. Brains were then transferred into 10% sucrose phosphate buffer (PB 0.1 M, pH 7.3) and stored overnight at 4 °C. Embedding was performed in a 12% gelatin/10% sucrose block, with fixation in 10% PFA/30% sucrose solution (PB 0.1 M, pH 7.3) for 2 h at room temperature and immersed in 30% sucrose (PB 0.1 M, pH 7.3) at 4 °C overnight. 40 um coronal sections were collected serially (rostral to caudal) using a freezing microtome (Leica; SM 2000R) and stored in PBS containing 0.2% Sodium azide.

For immunohistochemical analysis, sections were preincubated with a blocking PBS buffer containing 0.5% Triton X-100 and 10% normal horse serum (NHS; Invitrogen) for 1 h at room temperature. Sections were incubated in a mixture of primary antibodies in PBS buffer containing 0.4% Triton X-100 and 2% NHS for 72 h at 4 °C. The following primary antibodies

were used: rabbit antimCherry (1:500, Millipore, Abcam, ab167453), mouse anti-PV (1:1000, Swant, 235), and goat anti-MBP (1:300, Santa Cruz, C-16, sc-13 914).

Confocal imaging and reconstruction

Images were taken using a Zeiss LSM 700 microscope (Carl Zeiss) with 10x/0.45 NA, 40x/1.3 NA (oil immersion) and 63x/1.4 NA (oil immersion) objectives. Corresponding excitation wavelengths were used for Alexa488, Cy3 and Alexa647-secondary fluorophores (488 nm, 555 nm, and 639 nm, respectively). Biocytin-filled whole-cell overview image was acquired using 63x magnification objective with tiled *z*-stack images (512 × 512 pixels) with a step size of 1 µm. Three dimensional reconstruction of the cells was performed using the Neurolucida software(MBF Bioscience). Autapses were defined as individual sites where the distance between an axon and a dendrite of the same cell was less than 1 µm.

Quantification of region-dependent myelination was performed in the medial prefrontal cortex (mPFC) (bregma: + 2.10 to +1.54mm), by obtaining z stack images (1064 × 1064 pixels) at 63×magnification (1.4 NA; oil immersion) with 1× digital zoom at a step size of 1 µm. Immunofluorescent colocalization of MBP and tdTomato was manually counted using NIH ImageJ (version 1.41). At least 4 z-stacks were analyzed per mouse.

Social Behavior

The three chambers was performed in the sociability cage. Mice were first habituated for 5 minutes in the middle chamber and then 10 min with access to all three chambers empty, one day prior to testing. For the sociability test, the test mouse was first placed in the center chamber for 5 min with the doors closed. Then the doors were opened while a mouse of similar age and the same sex was kept under a wire cage in one of the side chambers (novel mouse). The other chamber contained an empty wire cage (novel object). The test mouse was left to freely explore the 3 chambers for 10 minutes. For the social novelty test, the test mouse was then placed back in the center chamber and the doors were closed again. A novel mouse was placed in the empty wire cage. The doors were then opened and the test mouse was again allowed to freely explore both mice for 10 min. Behavior was recorded and scored by Ethovision (Noldus: v.9,14). The time spent in each chamber was extracted and the percentage of time spent in the chamber was calculated as the total time spent in that chamber divided by the total time spent in all 3 chambers.

Statistical analysis

All statistical analysis were operated using GraphPad Prism 8. First, data were tested for normality. Data sets following normal distribution were analysed using unpaired two-tailed *t*-test. Data sets without a normal distribution were analysed using Mann Whitney test. One way ANOVA with LSD test for post-hoc analysis was used for group comparison for groups with

equal variances. Two-way repeated measures ANOVA was used for assessing effects within groups and between groups in experiments with repeated measurements in the same cell. All quantitative data are represented as means ± standard errors of the means (SEM). To reduce selection bias, all mice were randomly allocated to the different groups.

Acknowledgments

This work was funded in part by European Research Area Network ERA-NET NEURON JTC2018-024 / NWO 013.18.002 (M.P.G., S.A.K.) and ERA-PerMed2018-127 / ZonMw 456008003 (S.A.K.). We thank Nadia Pilati, Martin Gunthorpe, Martin Pue and Charles H. Large from Autifony S.r.l. for providing us with the Kv3 modulator AUT00201 and for their critical input on the subject; D. Slump for her assistance with breeding and genotyping of mice; D. Rotaru for her helpful suggestions; and all members of the Kushner laboratory for their support.

Author contributions

S.H. and S.K. contributed to the study design. S.H, M.P.G and Y.N contributed to data collection. S.H. carried on the data analysis. S.H., M.P.G., and S.K. wrote the paper. All authors discussed and commented on the manuscript.

Supplementary data

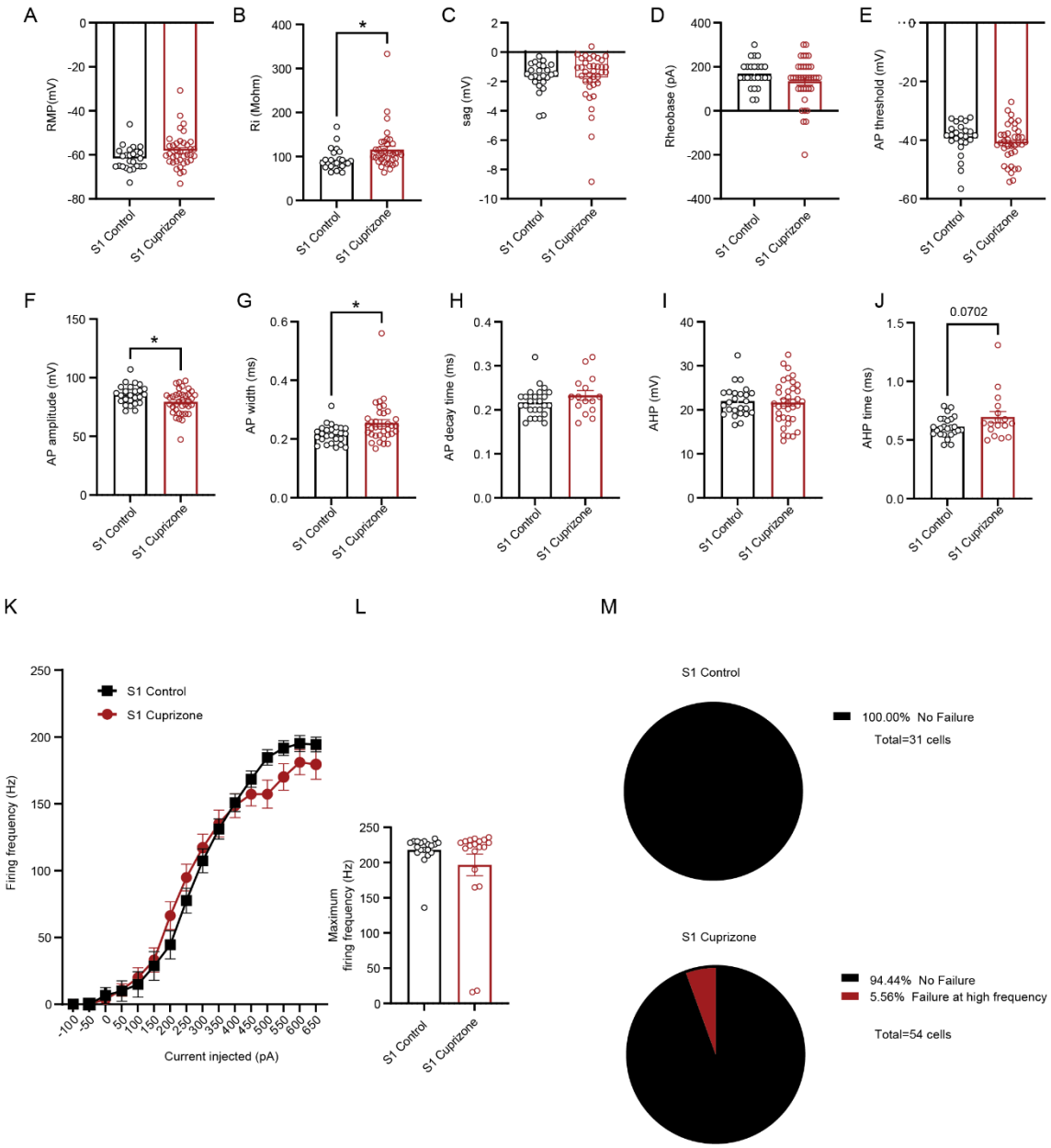

Supp. Figure 1. Effect of juvenile demyelination on intrinsic properties of S1 PV interneurons. A-J. Summary data showing the averaged (± s.e.m) of the following intrinsic properties: (A) Resting membrane potential (RMP) (*t-test; n = 25/37 cells from 8/9 mice per group, p = 0.0618*), (B) Input resistance (IR) (*t-test; n = 25/37 cells from 8/9 mice per group, *p = 0.0287*), (C) Sag (*t-test; n = 25/37 cells from 8/9 mice per group, p = 0.8511*), (D) Rheobase (*t-test; n = 25/37 cells from 8/9 mice per group, p = 0.1425*) and (E) Action potential (AP) threshold (*t-test; n = 25/37 cells from 8/9 mice per group, p = 0.2697*). (F) AP amplitude (*t-test; n = 25/37 cells from 8/9 mice per group, *p = 0.0173*), (G) AP half-width (*t-test; n = 25/37 cells from 8/9 mice per group, *p = 0.0134*), (H) AP decay (*t-test; n = 25/37 cells from 8/9 mice per group, p = 0.1996*), (I) After-hyperpolarization (AHP) amplitude (*t-test; n = 25/37 cells from 8/9 mice per group, p = 0.7570*) and (J) AHP time (*t-test; n = 25/37 cells from 8/9 mice per group, p = 0.0702*). **K**. Average action potential (AP) frequency in response to 0-650 pA current steps illustrating no significant change in S1 PV interneuron firing frequency following juvenile demyelination (*group x current mixed-effect analysis: n = 25/37 cells from 8/9 mice per group: p = 0.1036*). **L**. Summary data of the maximum firing frequency per group (*t-test; n = 25/37 cells from 8/9 mice per group, p = 0.8565*). **M**. Percentage of cells that failed to maintain high frequency firing at > 500 pA in both groups showing that in S1 almost none of the cells showed this failure.

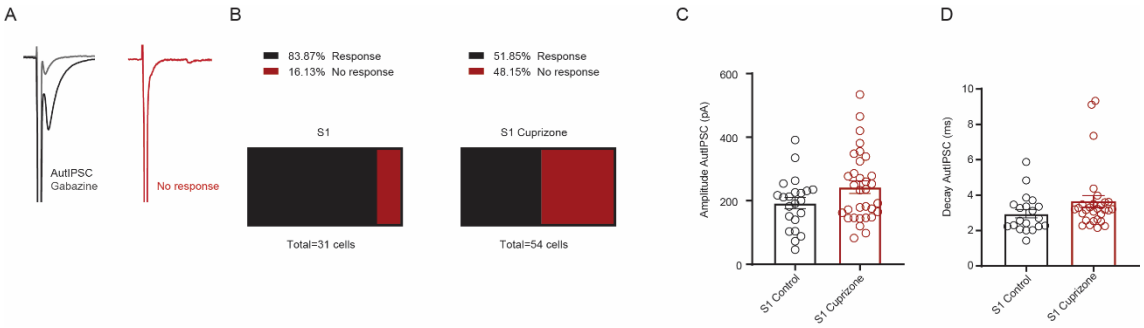

Supp. Figure 2. Effect of juvenile demyelination on autaptic neurotransmission in S1 PV interneurons. A. *Left*. Voltage steps from holding potential of- 70mV to 0 mV in PV interneuron induce fast inward Na+ currents (black, truncated), followed by slower inward inhibitory currents which can be blocked by gabazine (grey). *Right*. Traces from single trials showing a failure in autaptic response. **B**. Cuprizone-treated mice show a significant decrease in the percentage of S1 PV interneurons showing an autaptic response (*Fisher's exact test; **p = 0.0046*). **C**-**D**. There was no difference between groups in the amplitude (C) or decay (D) of the autaptic post-synaptic currents in cells that had autapses (*t-test; n = 22/32 cells from 8/9 mice per group, p = 0.0750 (C) and p = 0.1345 (D))*.

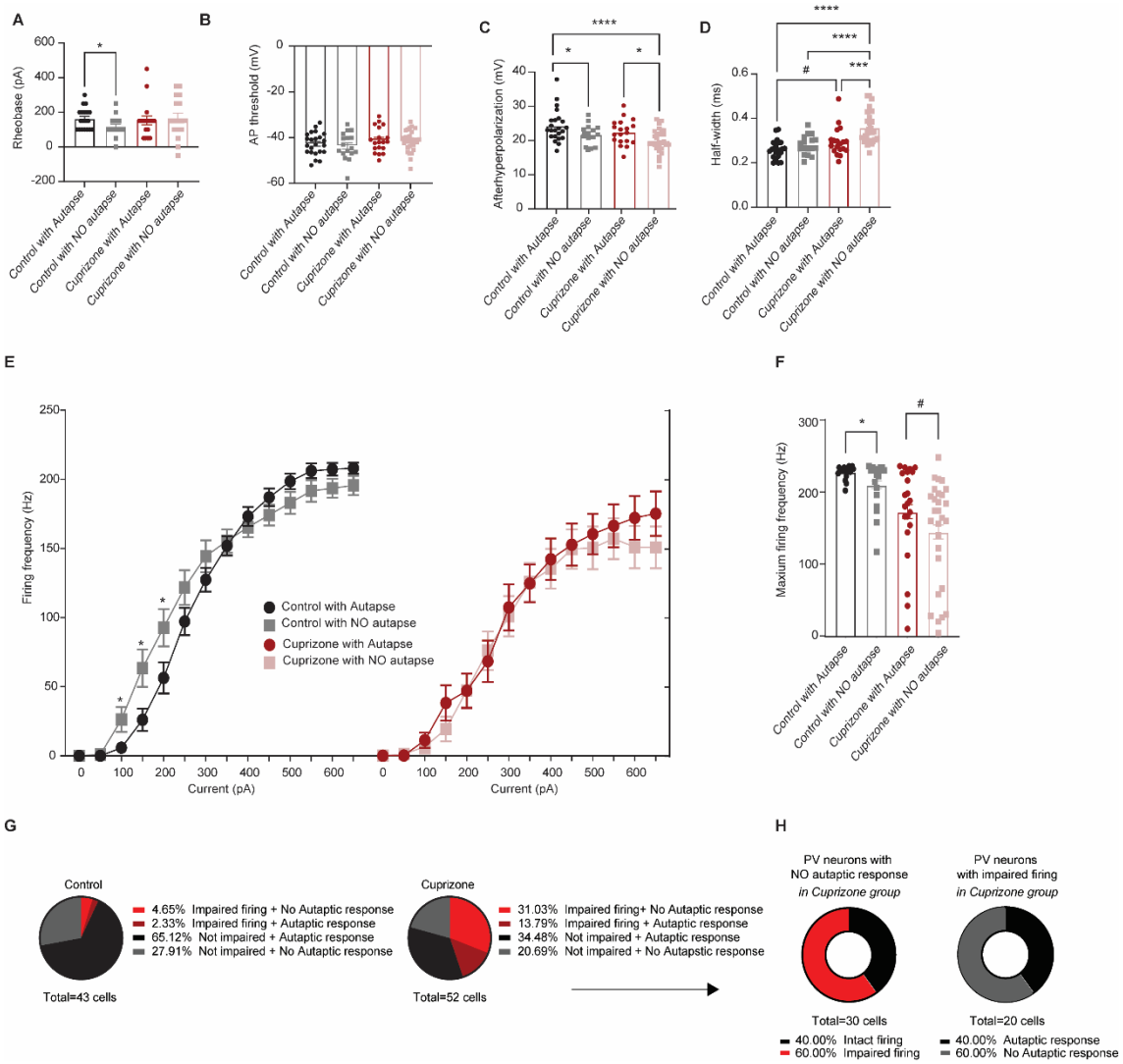

Supplementary Figure 3. Autapses play a crucial role in PV interneuron's sustained firing at high frequencies. A-F. Summary data of the averaged (± s.e.m) altered intrinsic properties of PV interneurons grouped by whether they show autaptic responses or not in both the control and the cuprizone-treated group: (**A**) Rheobase (*t-test of control with vs without autapse; n = 19 cells from 9 mice per group, *p < 0.01; t-test of cuprizone with vs without autapse; n = 17 cells from 8 mice per group, p = 0.6246*), (**B**) Action potential (AP) threshold (*t-test of control with vs without autapse; n = 19 cells from 9 mice per group, p = 0.5680; t-test of cuprizone with vs without autapse; n = 17 cells from 8 mice per group, p = 0.7648*), (**C**) After-hyperpolarization (AHP) amplitude (*ANOVA: n =19,19,18,18 cells from 9-8 mice per group, p = 0.0010, post-hoc LSD test: *p < 0.05, ****p < 0.0001*) and (**D**) AP half-width (*ANOVA: n =19,19,18,18 cells from 9-8 mice per group, p = 0.0002, post-hoc LSD test: #p = 0.0607 ***p < 0.001, ****p < 0.0001*). **E**. Average action potential (AP) frequency in response to 0-650 pA current steps illustrating a significant increase in PV interneuron firing frequency at low-current steps in control cells without autapses (grey) compared to control cells with autapses (black). Note that in cuprizone mice there was no difference (*group x current two-way repeated measures: n = 19,19,18,18 cells from 9-8 mice per group: F(39,856)= 1.671, p = 0.0068, post-hoc LSD test: *p < 0.05*). **F**. Summary data of the maximum firing frequency per group revealing a decrease in the maximum firing frequency in PV interneurons that do not have autapses (*t-test of control with vs without autapse; n = 19 cells from 9 mice per group, *p < 0.01; t-test of cuprizone with vs without autapse; n = 17 cells from 8 mice per group, p = 0.0722*). **G**. Pie chart showing the fraction of cells with impaired or intact firing and with or without autapses in both control mice (left) or cuprizone-treated mice (right). **H.** *Left.* Fraction of cells with intact or impaired firing within all the cells that had no autaptic response in the cuprizone group. *Right.* Fraction of cells with or without an autaptic response within all the cells that had impaired firing in the cuprizone group.

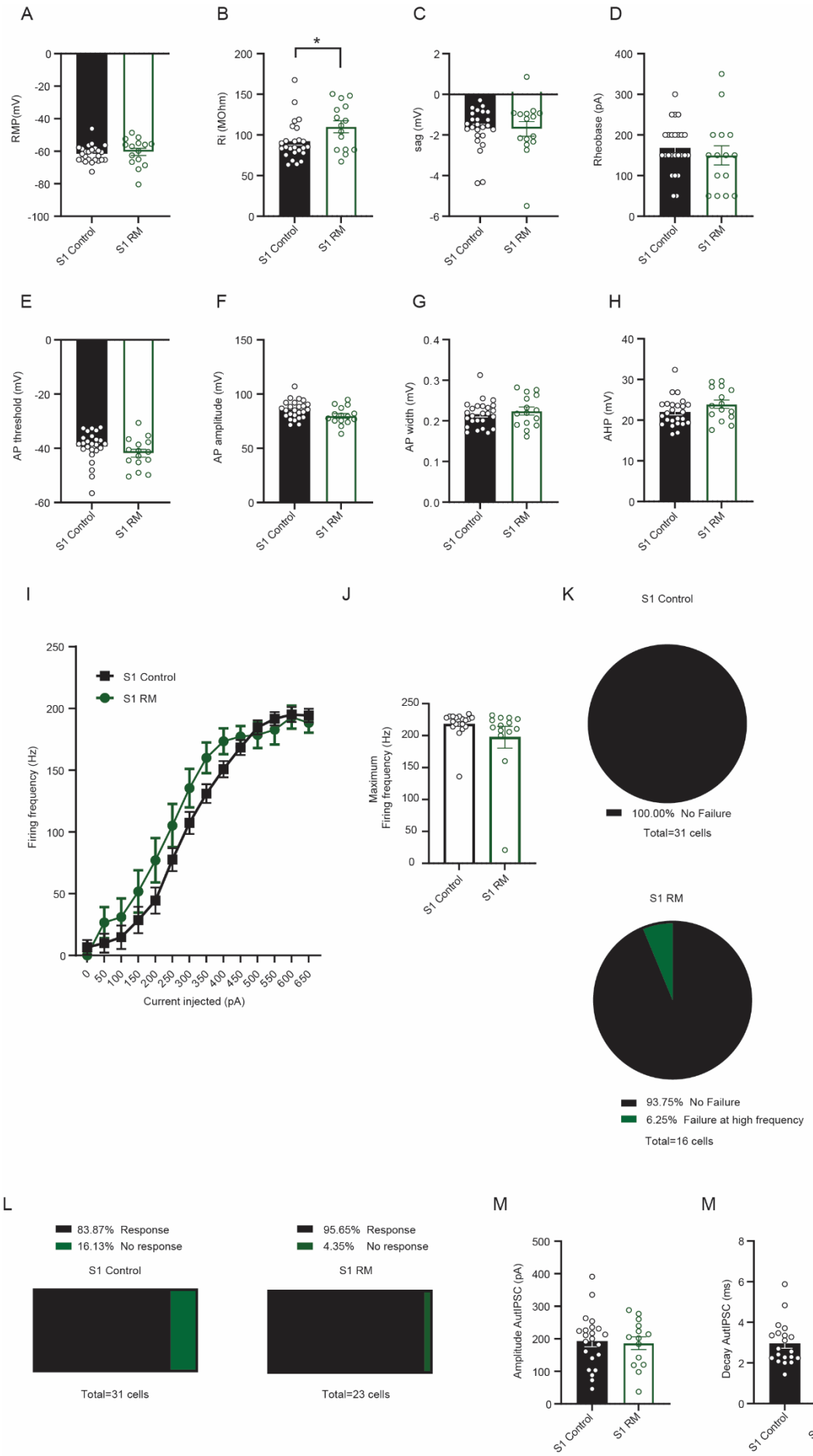
A
RMP(mV)
S1 Control
S1 RM
B
Ri (MOhm)
*
C
sag (mV)
D
Rheobase (pA)
E
AP threshold (mV)
F
AP amplitude (mV)
G
AP width (mV)
H
AHP (mV)
I
Firing frequency (Hz)
Current injected (pA)
J
Maximum Firing frequency (Hz)
K
S1 Control
100.00% No Failure
Total=31 cells
S1 RM
93.75% No Failure
6.25% Failure at high frequency
Total=16 cells
L
83.87% Response
16.13% No response
S1 Control
Total=31 cells
95.65% Response
4.35% No response
S1 RM
Total=23 cells
M
Amplitude AutIPSC (pA)
M
Decay AutIPSC (ms)

Supp. Figure 4. Remyelination can rescue PV properties in S1. A-H. Summary data showing the averaged (± s.e.m) of the following intrinsic properties: (A) Resting membrane potential (RMP) (*t-test; n = 25/15 cells from 8/5 mice per group, p = 0.5949*), (B) Input resistance (IR) (*t-test; n = 25/15 cells from 8/5 mice per group, *p = 0.0389*), (C) Sag (*t-test; n = 25/15 cells from 8/5 mice per group, p = 0.9429*), (D) Rheobase (*t-test; n = 25/15 cells from 8/5 mice per group, p = 0.4570*) and (E) Action potential (AP) threshold (*t-test; n = 25/15 cells from 8/5 mice per group, p = 0.1852*), (F) AP amplitude (*t-test; n = 25/15 cells from 8/5 mice per group, p = 0.0594*), (G) AP half-width (*t-test; n = 25/15 cells from 8/5 mice per group, p = 0.4887*) and (H) After-hyperpolarization (AHP) amplitude (*t-test; n = 25/15 cells from 8/5 mice per group, p = 0.1151*). **I**. Average action potential (AP) frequency in response to 0-650 pA current steps illustrating no significant change in S1 PV interneuron firing frequency following remyelination (*group x current mixed-effect analysis: n = 25/15 cells from 8/15 mice per group: p = 0.0638)*. **J**. Summary data of the maximum firing frequency per group (*t-test; n = 25/15 cells from 8/5 mice per group, p = 0.1775*). **K**. Percentage of cells that failed to maintain high frequency firing at > 500 pA in both groups showing that in S1 almost none of the cells showed impaired firing. **L.** Remyelination restores the percentage of cells showing an autaptic response in S1 PV interneurons. **M-N**. There was no difference between groups in the amplitude (M) or decay (N) of the autaptic post-synaptic currents in cells that had autapses (*t-test; n = 22/14 cells from 8/5 mice per group, p = 0.8164 (M) and p = 0.9172 (N).*

**p < 0.01*).

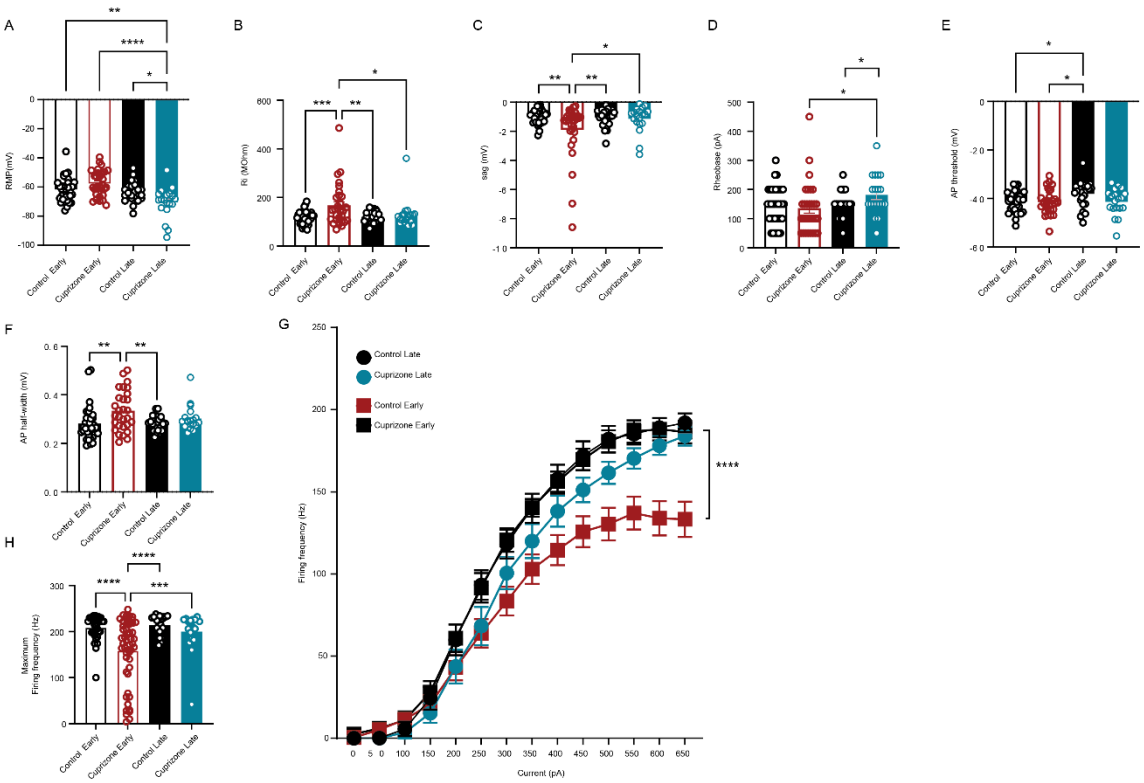

Supp. Figure 5. Comparison between juvenile and adult demyelination. A-I. Juvenile demyelination leads to impairment in PV interneuron maturation whereas adult demyelination induces a decrease in the excitability of PV interneurons. Summary data showing the averaged (± s.e.m) of the following intrinsic properties: (A) Resting membrane potential (RMP) (*ANOVA: n =36,30,19,24 cells from 9/8/8/6 mice per group, ****p < 0.0001, post-hoc LSD test: *p < 0.05, **p < 0.01, ****p < 0.0001*), (B) Input resistance (IR) (*ANOVA: n =36,30,19,24 cells from 9/8/8/6 mice per group, **p = 0.0024, post-hoc LSD test: *p < 0.05, **p < 0.01, ***p < 0.001*), (C) Sag (*ANOVA: n =36,30,19,24 cells from 9/8/8/6 mice per group, **p = 0.0083, post-hoc LSD test: *p < 0.05, **p < 0.01*), (D) Rheobase (*ANOVA: n =36,30,19,24 cells from 9/8/8/6 mice per group, p = 0.1230, post-hoc LSD test: *p < 0.05*) and (E) Action potential (AP) threshold (*ANOVA: n =36,30,19,24 cells from 9/8/8/6 mice per group, *p = 0.0452, post-hoc LSD test: *p*

< 0.05), (F) AP half-width (*ANOVA: n =36,30,19,24 cells from 9/8/8/6 mice per group, **p = 0.0058, post-hoc LSD test: **p < 0.01*), (G) Average action potential (AP) frequency in response to 0-650 pA current steps illustrating no significant change in S1 PV interneuron firing frequency following juvenile demyelination (*group x current two-way repeated measures: n = 36,30,19,24 cells from 9/8/8/6 mice per group: F(39,1291)= 2.487, ****p < 0.0001*) and (H) Maximum firing frequency per group (*ANOVA: n =36,30,19,24 cells from 9/8/8/6 mice per group, ****p < 0.0001, post-hoc LSD test: ***p < 0.001, ****p < 0.0001*).

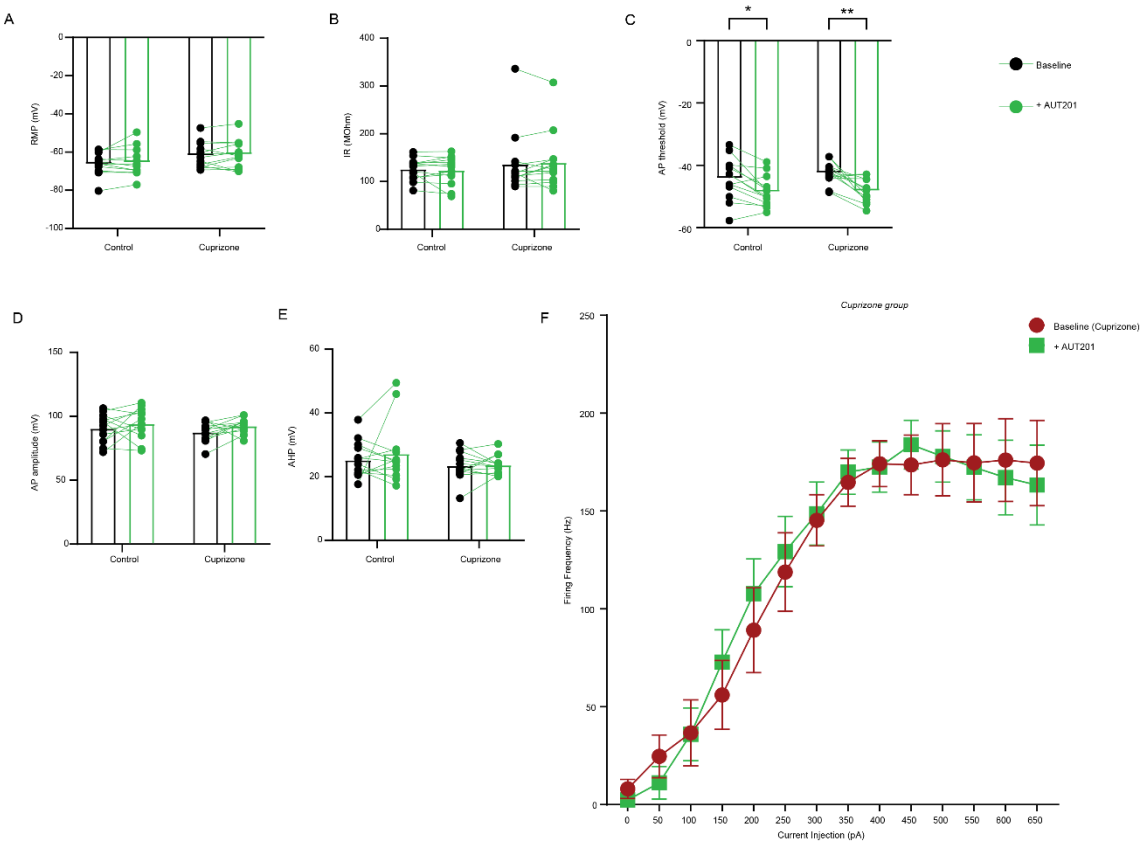

Supp. Figure 6. Effect of AUT00201 (1uM) on PV properties after juvenile demyelination. A-B. Bath application of AUT00201 (1uM) had no significant effect on the resting membrane potential (A) or the input resistance (B) of PV interneurons from cuprizone mice and control mice (RMP: *group x AUT00201 two-way repeated measures: n = 12,13 cells from 4 mice per group: p = 0.8593; AUT00201 effect: p = 0.2171*. IR: *group x AUT00201: p = 0.8605; AUT00201 effect: p = 0.4704*). **C**-**E**. AUT00201 decreased the AP threshold of PV interneurons in both groups (*group x AUT00201 two-way repeated measures: n = 12,13 cells from 4 mice per group: p = 0.4503; AUT00201 effect: ****p < 0.0001. Post-hoc LSD analysis: *p < 0.05, **p < 0.01*) while not having an effect on either the AP amplitude (D) or the AHP (E) (D: *group x AUT00201 two-way repeated measures: n = 12,13 cells from 4 mice per group: p = 0.8235; AUT00201 effect: p = 0.0763*. E: *group x AUT00201: p = 0.6088; AUT00201 effect: p = 0.3628*. **F**. There was no effect detected on the overall firing frequency of PV interneurons from cuprizone-treated mice after bath application of AUT00201 when averaging all the cells together (*group x current two-way repeated measures: n = 13 cells from 4 mice per group: F(13,78)= 0.9280, p = 0.5287. AUT00201 effect: F(1,6)= 5.05, p = 0.0657*).

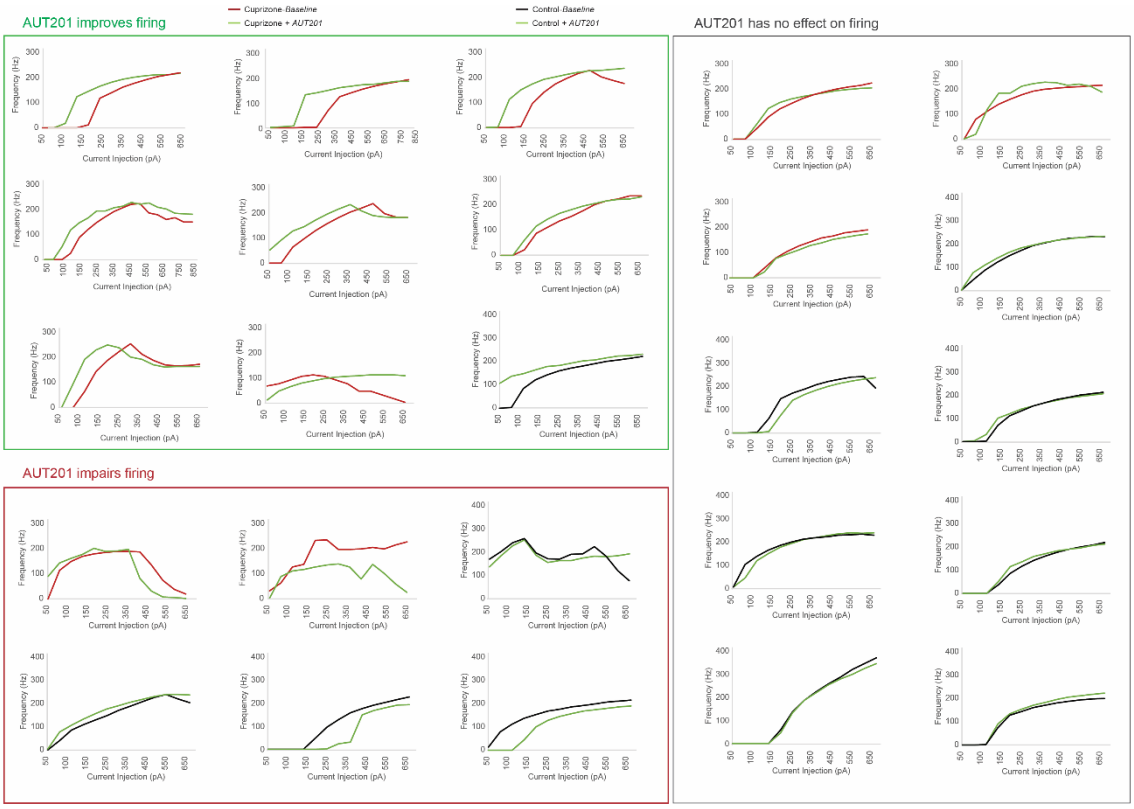

Supp. Figure 7. Effect of KV3 modulation on PV interneuron firing frequency and on autaptic release. Effect of bath application of AUT00201 (1uM) (green) on the firing frequency of individual PV interneurons in control (black) and cuprizone-treated (red) mice. The cells were divided into 3 groups: AUT00201 improved the firing, impaired the firing or had no effect.

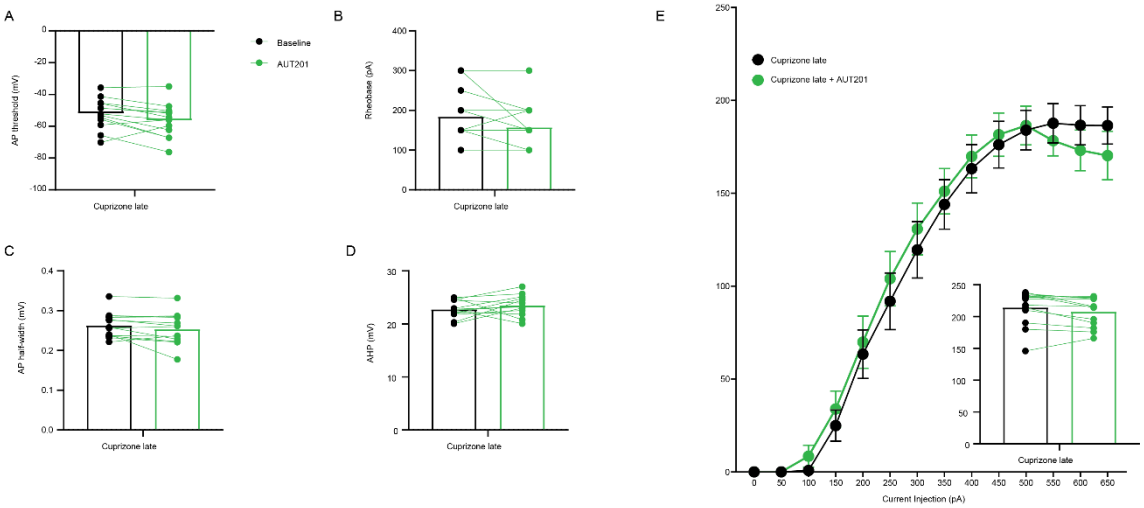

Supp. Figure 8. Effect of AUT00201 (1uM) on PV properties after adult demyelination. A-E. Bath application of AUT00201 (1uM) had no significant effect on any of the intrinsic properties of PV interneurons following adult demyelination. Summary data showing the averaged (± s.e.m) of the AP threshold (A) , the rheobase (B) , the AP half-width (C), the AHP (D) and the overall firing frequency of PV interneurons from mice that underwent adult demyelination (E) (*Paired t-test:* A: $p = 0.1006$, B: $p = 0.0678$, C: $p = 0.1006$, D: $p = 0.2812$, E: $p = 0.0653$; *two-way repeated measures: AUT00201 effect:* $F(1,12)= 0.4990$, $p = 0.4934$).

References

1. Goldberg, E. M. *et al.* Rapid developmental maturation of neocortical FS cell intrinsic excitability. *Cereb Cortex* **21**, 666–682 (2011).
2. Daw, M. I., Ashby, M. C. & Isaac, J. T. R. Coordinated developmental recruitment of latent fast spiking interneurons in layer IV barrel cortex. *Nat Neurosci* **10**, 453–461 (2007).
3. Micheva, K. D., Kiraly, M., Perez, M. M. & Madison, D. V. Extensive Structural Remodeling of the Axonal Arbors of Parvalbumin Basket Cells during Development in Mouse Neocortex. *J Neurosci* **41**, 9326–9339 (2021).
4. Micheva, K. D. *et al.* A large fraction of neocortical myelin ensheathes axons of local inhibitory neurons. *Elife* **5**, e15784 (2016).
5. Stedehouder, J. *et al.* Fast-spiking Parvalbumin Interneurons are Frequently Myelinated in the Cerebral Cortex of Mice and Humans. *Cereb Cortex* **27**, 5001–5013 (2017).
6. Micheva, K. D., Kiraly, M., Perez, M. M. & Madison, D. V. Conduction Velocity Along the Local Axons of Parvalbumin Interneurons Correlates With the Degree of Axonal Myelination. *Cereb Cortex* **31**, 3374–3392 (2021).
7. Benamer, N., Vidal, M., Balia, M. & Angulo, M. C. Myelination of parvalbumin interneurons shapes the function of cortical sensory inhibitory circuits. *Nat Commun* **11**, 5151 (2020).
8. Dubey, M. *et al.* Myelination synchronizes cortical oscillations by consolidating parvalbumin-mediated phasic inhibition. *Elife* **11**, e73827 (2022).
9. Fang, L.-P. *et al.* Impaired bidirectional communication between interneurons and oligodendrocyte precursor cells affects social cognitive behavior. *Nat Commun* **13**, 1394 (2022).
10. Stedehouder, J. & Kushner, S. A. Myelination of parvalbumin interneurons: a parsimonious locus of pathophysiological convergence in schizophrenia. *Mol Psychiatry* **22**, 4–12 (2017).
11. Leicht, G. *et al.* EEG-Informed fMRI Reveals a Disturbed Gamma-Band-Specific Network in Subjects at High Risk for Psychosis. *Schizophr Bull* **42**, 239–249 (2016).
12. van Os, J. & Kapur, S. Schizophrenia. *Lancet* **374**, 635–645 (2009).
13. Chini, M. & Hanganu-Opatz, I. L. Prefrontal Cortex Development in Health and Disease: Lessons from Rodents and Humans. *Trends Neurosci* **44**, 227–240 (2021).
14. Bicks, L. K. *et al.* Prefrontal parvalbumin interneurons require juvenile social experience to establish adult social behavior. *Nat Commun* **11**, 1003 (2020).
15. Klune, C. B., Jin, B. & DeNardo, L. A. Linking mPFC circuit maturation to the developmental regulation of emotional memory and cognitive flexibility. *Elife* **10**, e64567 (2021).
16. Coley, A. A., Padilla-Coreano, N., Patel, R. & Tye, K. M. Valence processing in the PFC: Reconciling circuit-level and systems-level views. *Int Rev Neurobiol* **158**, 171–212 (2021).
17. Bitzenhofer, S. H., Pöpplau, J. A., Chini, M., Marquardt, A. & Hanganu-Opatz, I. L. A transient developmental increase in prefrontal activity alters network maturation and causes cognitive dysfunction in adult mice. *Neuron* **109**, 1350-1364.e6 (2021).
18. Deleuze, C. *et al.* Strong preference for autaptic self-connectivity of neocortical PV interneurons facilitates their tuning to γ-oscillations. *PLoS Biol* **17**, e3000419 (2019).
19. Deleuze, C., Pazienti, A. & Bacci, A. Autaptic self-inhibition of cortical GABAergic neurons: Synaptic narcissism or useful introspection? *Current Opinion in Neurobiology* **26**, 64–71 (2014).
20. Szegedi, V. *et al.* Robust perisomatic GABAergic self-innervation inhibits basket cells in the human and mouse supragranular neocortex. *Elife* **9**, e51691 (2020).
21. Connelly, W. M. & Lees, G. Modulation and function of the autaptic connections of layer V fast spiking interneurons in the rat neocortex. *The Journal of Physiology* **588**, 2047–2063 (2010).
22. Makinodan, M., Rosen, K. M., Ito, S. & Corfas, G. A Critical Period for Social Experience–Dependent Oligodendrocyte Maturation and Myelination. *Science* **337**, 1357–1360 (2012).

23. Miyamae, T., Chen, K., Lewis, D. A. & Gonzalez-Burgos, G. Distinct Physiological Maturation of Parvalbumin-Positive Neuron Subtypes in Mouse Prefrontal Cortex. *J. Neurosci.* **37**, 4883–4902 (2017).
24. Johnston, J., Forsythe, I. D. & Kopp-Scheinpflug, C. SYMPOSIUM REVIEW: Going native: voltage-gated potassium channels controlling neuronal excitability: K^+ channels and auditory processing. *The Journal of Physiology* **588**, 3187–3200 (2010).
25. Rosato-Siri, M. D. *et al.* A Novel Modulator of Kv3 Potassium Channels Regulates the Firing of Parvalbumin-Positive Cortical Interneurons. *J Pharmacol Exp Ther* **354**, 251–260 (2015).
26. Bacci, A., Huguenard, J. R. & Prince, D. A. Functional Autaptic Neurotransmission in Fast-Spiking Interneurons: A Novel Form of Feedback Inhibition in the Neocortex. *J. Neurosci.* **23**, 859–866 (2003).
27. Yang, S. M., Michel, K., Jokhi, V., Nedivi, E. & Arlotta, P. Neuron class–specific responses govern adaptive myelin remodeling in the neocortex. *Science* **370**, eabd2109 (2020).
28. Maas, D. A. *et al.* Interneuron hypomyelination is associated with cognitive inflexibility in a rat model of schizophrenia. *Nat Commun* **11**, 2329 (2020).
29. Toritsuka, M., Makinodan, M. & Kishimoto, T. Social Experience-Dependent Myelination: An Implication for Psychiatric Disorders. *Neural Plasticity* **2015**, 1–6 (2015).
30. Makinodan, M. *et al.* Demyelination in the juvenile period, but not in adulthood, leads to long-lasting cognitive impairment and deficient social interaction in mice. *Progress in Neuro-Psychopharmacology and Biological Psychiatry* **33**, 978–985 (2009).
31. Yang, Y. *et al.* Neonatal Maternal Separation Impairs Prefrontal Cortical Myelination and Cognitive Functions in Rats Through Activation of Wnt Signaling. *Cereb. Cortex* bhw121 (2016) doi:10.1093/cercor/bhw121.
32. Zendedel, A., Beyer, C. & Kipp, M. Cuprizone-Induced Demyelination as a Tool to Study Remyelination and Axonal Protection. *J Mol Neurosci* **51**, 567–572 (2013).
33. Gingele, S. *et al.* Delayed Demyelination and Impaired Remyelination in Aged Mice in the Cuprizone Model. *Cells* **9**, 945 (2020).
34. Hiremath, M. M. *et al.* Microglial/macrophage accumulation during cuprizone-induced demyelination in C57BL/6 mice. *Journal of Neuroimmunology* **92**, 38–49 (1998).
35. De- and remyelination in the CNS white and grey matter induced by cuprizone: The old, the new, and the unexpected. *Histology and Histopathology* 1585–1597 (2011) doi:10.14670/HH-26.1585.
36. Hamada, M. S. & Kole, M. H. P. Myelin Loss and Axonal Ion Channel Adaptations Associated with Gray Matter Neuronal Hyperexcitability. *Journal of Neuroscience* **35**, 7272–7286 (2015).
37. Kourdougli, N. *et al.* Improvement of sensory deficits in fragile X mice by increasing cortical interneuron activity after the critical period. *Neuron* S0896627323004683 (2023) doi:10.1016/j.neuron.2023.06.009.
38. Roth, F. C. & Hu, H. An axon-specific expression of HCN channels catalyzes fast action potential signaling in GABAergic interneurons. *Nat Commun* **11**, 2248 (2020).
39. Goldberg, E. M. Specific Functions of Synaptically Localized Potassium Channels in Synaptic Transmission at the Neocortical GABAergic Fast-Spiking Cell Synapse. *Journal of Neuroscience* **25**, 5230–5235 (2005).
40. Bitzenhofer, S. H., Pöpplau, J. A. & Hanganu-Opatz, I. Gamma activity accelerates during prefrontal development. *eLife* **9**, e56795 (2020).